Journal of Computational Physics 546 (2026) 114511

Contents lists available at ScienceDirect

Journal of Computational Physics

journal homepage: www.elsevier.com/locate/jcp

Path-conservative finite volume scheme with Hooke's law-preserving paths for non-conservative hyperbolic system of hypo-elastic plastic solid

Zhiqiang Zeng [a], Hao Wang [a], Tiegang Liu [a], Changsheng Yu [b,*]

[a] LMIB and School of Mathematical Sciences, Beihang University, Beijing, PR China
[b] Institute of Mathematics, Johannes Gutenberg-University Mainz, Staudingerweg 9, 55128, Mainz, Germany

ARTICLE INFO

Keywords:
Elastic plastic solid
Path-conservative scheme
Hooke's law
Riemann solver

ABSTRACT

In this paper, we propose a path-conservative finite volume scheme to address the non-conservative nature of governing equations for hypo-elastic plastic solids. By combining the Hooke's law-preserving path with the Riemann solver, a novel class of piecewise paths is proposed. Furthermore, we process the model changes during elastic-plastic transitions by incorporating deviatoric stress iteration, establishing transition formulas, and formulating the elastic-plastic interface fluxes. Our method has been applied to both one-dimensional and two-dimensional elastic-plastic solid models. Numerical tests have demonstrated its effectiveness.

1. Introduction

The advancements in weapon physics, particularly in areas such as ship damage assessment, armor penetration, and inertial confinement nuclear fusion, have driven significant research into elastic-plastic solids, for example [1–13]. Among the various elastic-plastic solid models, the hypo-elastic plastic model has gained considerable attention due to its numerical results closely matching experimental data. These physical scenarios often involve strong impacts, and given the non-conservative nature of the stress equations in the hypo-elastic plastic model, careful attention must be paid to the construction of its discrete method to avoid non-physical numerical results [14].

Within the framework of the finite volume method, there are two common approaches to handling non-conservative terms: the quasi-conservative scheme [15–18] and the path-conservative scheme [19–22]. The path-conservative method, derived from the DLM theory (Dal Maso-LeFloch-Murat) that characterizes weak solutions through a family of paths in phase space, relies on a prescribed set of paths to obtain the numerical flux. For the system of fluid dynamics, numerous researchers have proposed various path-conservative discrete methods, e.g., [19,23–27]. However, that method has not received much attention for elastic-plastic solids, leaving a gap in the research. There are two underlying issues: constructing a physically consistent path (i.e., Hooke's law) and handling elastic-plastic transitions.

The first issue arises from the fact that the governing equations for hypo-elastic solids include not only the conservation of mass and momentum but also non-conservative stress equations derived from Hooke's law. While multiple path selections are theoretically admissible, see [28], different choices lead to divergent shock wave solutions. To maintain consistency with Hooke's law across the shock wave, the path specification becomes imperative. The second issue concerns the transition between the elastic solid model and

* Corresponding author.
E-mail address: chayu@uni-mainz.de (C. Yu).

https://doi.org/10.1016/j.jcp.2025.114511
Received 8 April 2025; Received in revised form 26 September 2025; Accepted 4 November 2025
Available online 19 November 2025

the plastic solid model, which is governed by the von Mises yield condition, see [29]. The two models differ fundamentally: the elastic model incorporates stress equations, while the plastic model replaces them with energy equations. Moreover, the von Mises stress condition depends on the deviatoric stress, yet the deviatoric stress constitutes only part of the total stress and does not explicitly appear in the governing equations, see [30]. All these factors significantly complicate the numerical treatment of elastic-plastic transitions.

Based on the preceding discussion, this paper first proposes a specific path and proves that the resulting shock waves still satisfy Hooke's law. Subsequently, through Riemann solvers–including a novel linearized shock wave Riemann solver–we derive generalized piecewise paths and obtain the corresponding numerical fluxes. We complete the numerical treatment of elastic-plastic transitions by introducing deviatoric stress iteration into the numerical scheme, providing transition formulas for model switching, and formulating numerical fluxes at elastic-plastic interfaces. The proposed method has been applied to both one-dimensional and two-dimensional elastic-plastic models, yielding corresponding path-conservative numerical schemes whose effectiveness is demonstrated through numerical tests.

This paper is arranged as follows. In Section 2, the governing equations for one-dimensional elastic-plastic solids are introduced, along with the weak solution in the sense of DLM theory. In Section 3, the paths and Riemann solvers for hypo-elastic solid model are introduced. In Section 4, we present the path-conservative finite volume scheme for non-conservative hyperbolic system of hypo-elastic plastic solid. Section 5 extends the one-dimensional method to two dimensions. Section 6 extends the two-dimensional work to include the Jaumann correction. Section 7 presents several numerical examples to validate the proposed method. Finally, Section 8 provides a breif conclusion.

2. One-dimensional elastic-plastic solid model

2.1. Hypo-elastic solid

The governing equation for the hypo-elastic solid is

$$\frac{\partial \mathbf{W}}{\partial t} + \frac{\partial \mathbf{F}^e(\mathbf{W})}{\partial x} = \mathbf{S}(\mathbf{W}) \tag{2.1}$$

with

$$\mathbf{W} = \begin{pmatrix} \rho \\ \rho u \\ \rho\sigma \end{pmatrix},\ \mathbf{F}^e(\mathbf{W}) = \begin{pmatrix} \rho u \\ \rho u^2 - \sigma \\ \rho u \sigma \end{pmatrix},\ \mathbf{S}(\mathbf{W}) = \begin{pmatrix} 0 \\ 0 \\ \rho\left(K + \frac{4}{3}\mu\right)\frac{\partial u}{\partial x} \end{pmatrix}. \tag{2.2}$$

Here ρ is the density, u is the velocity, σ is the total stress , K is the bulk modulus and μ is the shear modulus. In the rest of this paper, we tacitly assume that the density is always positive, both in the analysis and the numerical scheme. This assumption is reasonable for solids. The total stress σ can be decomposed into the hydrostatic pressure p and the deviatoric stress s:

$$\sigma = -p + s. \tag{2.3}$$

Here and after, the uppercase superscript "e" is a mnemonic symbol to help indicate the elastic state. The elastic solid should satisfy the Mises yield condition $s^2 \le \left(\frac{2}{3}Y_0\right)^2$, and Y_0 is the yield strength of the material in simple tension. Eq. (2.1) can be written in the following quasi-linear form

$$\frac{\partial \mathbf{W}}{\partial t} + \mathbf{A}(\mathbf{W})\frac{\partial \mathbf{W}}{\partial x} = 0 \tag{2.4}$$

with

$$\mathbf{A}(\mathbf{W}) = \frac{\partial \mathbf{F}^e(\mathbf{W})}{\partial \mathbf{W}} + \begin{pmatrix} 0 & 0 & 0 \\ 0 & 0 & 0 \\ \left(\frac{4}{3}\mu + K\right)u & -\left(\frac{4}{3}\mu + K\right) & 0 \end{pmatrix}. \tag{2.5}$$

The eigenvalues of the Eq. (2.4) are

$$\lambda_1^e(\mathbf{W}) = u - c^e, \quad \lambda_2^e(\mathbf{W}) = u, \quad \lambda_3^e(\mathbf{W}) = u + c^e \tag{2.6}$$

with $c^e = \sqrt{\frac{4\mu+3K}{3\rho}} > 0$. The corresponding right eigenvectors are

$$\mathbf{R}_1^e(\mathbf{W}) = \begin{pmatrix} -\rho \\ c^e \\ -(c^e)^2\rho \end{pmatrix},\quad \mathbf{R}_2^e(\mathbf{W}) = \begin{pmatrix} 1 \\ 0 \\ 0 \end{pmatrix},\quad \mathbf{R}_3^e(\mathbf{W}) = \begin{pmatrix} \rho \\ c^e \\ (c^e)^2\rho \end{pmatrix}. \tag{2.7}$$

It is easy to show that both the λ_1^e-field and λ_3^e-field are genuinely nonlinear, and the λ_2^e-field is linearly degenerate:

$$\nabla\lambda_1^e \cdot \mathbf{R}_1 \neq 0, \quad \nabla\lambda_2^e \cdot \mathbf{R}_2 = 0, \quad \nabla\lambda_3^e \cdot \mathbf{R}_3 \neq 0.$$

2.2. Perfectly plastic solid

The governing equation for the perfectly plastic solid is

$$\frac{\partial \mathbf{U}}{\partial t}+\frac{\partial \mathbf{F}^p(\mathbf{U})}{\partial x}=0,\ \mathbf{U}=\begin{pmatrix}\rho\\ \rho u\\ E\end{pmatrix},\ \mathbf{F}^p(\mathbf{U})=\begin{pmatrix}\rho u\\ \rho u^2-\sigma\\ (E-\sigma)u\end{pmatrix}. \tag{2.8}$$

The uppercase superscript "p" is a mnemonic symbol to help indicate the plastic state. ρ is the density, u is the velocity, σ is the total stress, and E is the total energy. The total energy per unit volume is given by $E=\rho e+\frac{1}{2}\rho u^2$, where e represents the specific internal energy. In addition, the deviatoric stress s for the plastic solid is treated as a constant owing to the perfectly plastic assumption. An appropriate constitutive model must be incorporated to ensure the closure of systems (2.8). In this paper, the following constitutive model is used:

(i) total stress decomposition: $\sigma=-p+s$;
(ii) perfectly plastic assumption: stresses are rescaled by multiplying: $s=\pm\frac{2}{3}Y_0$;
(iii) stiffened-gas equation of state: $p=c_0^2(\rho-\rho_0)+(\gamma-1)\rho e$.

Here c_0 and ρ_o are the reference sound speed and the reference density, respectively. γ is the Grüneisen parameter. The eigenvalues of the system (2.8) and their corresponding right eigenvectors are

$$\lambda_1^p(\mathbf{U})=u-c^p,\ \lambda_2^p(\mathbf{U})=u,\ \lambda_3^p(\mathbf{U})=u+c^p, \tag{2.9}$$

and

$$\mathbf{R}_1^p(\mathbf{U})=\begin{pmatrix}-\rho\\ c^p\\ -(c^p)^2\rho\end{pmatrix},\quad \mathbf{R}_2^p(\mathbf{U})=\begin{pmatrix}1\\0\\0\end{pmatrix},\quad \mathbf{R}_3^p(\mathbf{U})=\begin{pmatrix}\rho\\ c^p\\ \mp(c^p)^2\rho\end{pmatrix} \tag{2.10}$$

with

$$c^p=\sqrt{\left(\gamma p^p+c_0^2\rho_0-(\gamma-1)s\right)/\rho}.$$

The λ_2^p-field is linearly degenerate, and both λ_1^p-field and λ_3^p-field are genuinely nonlinear:

$$\nabla\lambda_1^p\cdot\mathbf{R}_1\neq 0,\quad \nabla\lambda_2^p\cdot\mathbf{R}_2=0,\quad \nabla\lambda_3^p\cdot\mathbf{R}_3\neq 0.$$

2.3. Weak solution

Let us consider a non-conservative hyperbolic equation

$$\partial_t\mathbf{W}+\mathbf{A}(\mathbf{W})\partial_x\mathbf{W}=0,\quad x\in\boldsymbol{R},\ t>0, \tag{2.11}$$

where $\mathbf{W}(x,t)$ belongs to an open convex set. It is assumed that the system (2.11) is strictly hyperbolic, meaning that the matrix $\mathbf{A}(\mathbf{W})$ possesses N distinct real eigenvalues $\lambda_1(\mathbf{W})<\ldots<\lambda_N(\mathbf{W})$. The corresponding eigenvectors, denoted as $R_1(\mathbf{W}),\ldots,R_N(\mathbf{W})$, are associated with these eigenvalues. Furthermore, the characteristic fields $R_1(\mathbf{W}),\ldots,R_N(\mathbf{W})$ are presumed to be either genuinely nonlinear or linearly degenerate.

The DLM theory developed by Dal Maso, LeFloch, and Murat in [31] can define the weak solutions for non-conservative systems (2.11) with a family of paths.

Definition 2.1. *A family of paths in Ω is a local Lipschitz map*

$$\Phi:[0,1]\times\Omega\times\Omega\mapsto\Omega$$

such that

(1) $\Phi(0;\mathbf{W}_L,\mathbf{W}_R)=W_L$ and $\Phi(1;\mathbf{W}_L,\mathbf{W}_R)=U_R$ for any $\mathbf{W}_L,\mathbf{W}_R\in\Omega$;
(2) for every arbitrary bounded set $O\subset\Omega$, there exists a constant k such that

$$\left|\frac{\partial\Phi}{\partial s}(s;\mathbf{W}_L,\mathbf{W}_R)\right|\le k|\mathbf{W}_R-\mathbf{W}_L|,$$

for any $\mathbf{W}_L,\mathbf{W}_R\in O$ and almost every $s\in[0,1]$;
(3) for every bounded set $O\in\Omega$, there exists a constant K such that

$$\left|\frac{\partial\Phi}{\partial s}(s;\mathbf{W}_L^1,\mathbf{W}_R^1)-\frac{\partial\Phi}{\partial s}(s;\mathbf{W}_L^2,\mathbf{W}_R^2)\right|\le K\left(\left|\mathbf{W}_L^1-\mathbf{W}_L^2\right|+\left|\mathbf{W}_R^1-\mathbf{W}_R^2\right|\right)$$

for any $\mathbf{W}_L^1,\mathbf{W}_R^1,\mathbf{W}_L^2,\mathbf{W}_R^2\in\mathcal{O}$ and almost every $s\in[0,1]$.

For a given family of paths Φ, the non-conservative product $\mathbf{A}(\mathbf{W})\mathbf{W}_x$ can be interpreted as a Borel measure $\left[\mathbf{A}(\mathbf{W})\mathbf{W}_x\right]_\Phi$, whose Lebesgue decomposition is $\mu_a^\Phi + \mu_s^\Phi$ and

$$\mu_a^\Phi = \int_E \mathbf{A}(\mathbf{W}(x,t))\mathbf{W}_x(x,t)\phi(x)\mathrm{d}x$$

for every Borel set E, and

$$\mu_s^\Phi = \sum_l \left(\int_0^1 \mathbf{A}\left(\Phi\left(s;\mathbf{W}_l^-,\mathbf{W}_l^+\right)\right)\frac{\partial \Phi}{\partial s}\left(s;\mathbf{W}_l^-,\mathbf{W}_l^+\right)\mathrm{d}s \right)\delta_{x_l(t)},$$

where $\mathbf{W}$ is discontinuous at the location $x_l(t)$ with left-hand state $\mathbf{W}_l^-$ and right-hand state $\mathbf{W}_l^+$, and $\delta_{x_l(t)}$ is the Dirac measure placed at $x_l(t)$. For a given family of paths Φ, the weak solution $\mathbf{W} \in L^\infty\left(\boldsymbol{R}\times\boldsymbol{R}^+\right) \cap BV\left(\boldsymbol{R}\times\boldsymbol{R}^+\right)$ is a piecewise C^1 function and defined by

$$\langle \mathbf{W}_t, \phi\rangle + \left\langle \left[\mathbf{A}(\mathbf{W})\mathbf{W}_x\right]_\Phi, \phi\right\rangle = 0, \quad \forall \phi \in C_0^\infty(\boldsymbol{R}), \tag{2.12}$$

where $C_0^\infty(\boldsymbol{R})$ is the set of continuous functions with compact support. The discontinuity in the weak solution between left-hand state $\mathbf{W}^-$ and right-hand state $\mathbf{W}^+$ moving at speed ς must satisfy the generalized Rankine-Hugoniot condition

$$\int_0^1 \left(\varsigma \mathcal{I} - \mathbf{A}\left(\Phi\left(s;\mathbf{W}^-,\mathbf{W}^+\right)\right)\right)\frac{\partial \Phi}{\partial s}\left(s;\mathbf{W}^-,\mathbf{W}^+\right)ds = 0, \tag{2.13}$$

where $\mathcal{I}$ is the identity matrix.

3. Path for hypo-elastic solid model

3.1. Path for elastic waves

The path chosen affects the travel speed of the shock wave and is therefore critical. In this section, we consider the path of a shock wave in the elastic model. Suppose a discontinuity with the left-hand state $\mathbf{W}_L$ and the right-hand state $\mathbf{W}_R$ in the weak solution. We will sepecify a path and derive the jump relation between $\mathbf{W}_L$ and $\mathbf{W}_R$. We use the standard average and jump operators for any two quantities w_L and w_R as follows.

$$\{\{w\}\} = \frac{w_L + w_R}{2}, \ [\![w]\!] = w_R - w_L.$$

We observe that the nonconserved products in the hypo-elastic model involve only the derivatives of velocity, therefore we only need to give the paths of ρ and m. We use linear paths for both density and momentum, as follows.

$$\begin{cases} \rho\left(s;U_L,U_R\right) = \rho_L + s(\rho_R - \rho_L), \\ m\left(s;U_L,U_R\right) = m_L + s(m_R - m_L). \end{cases} \tag{3.1}$$

In general, a suitable path should be derived from a viscous process. In the following sections, we will demonstrate that this linear path ensures the validity of Hooke's law within the elastic solid model.

Let us use the notation

$$\widetilde{\rho}_{L,R} = \begin{cases} \rho_L\rho_R\frac{[\![\ln\rho]\!]}{[\![\rho]\!]}, & \rho_L \neq \rho_R \\ \rho_L, & \rho_L = \rho_R \end{cases}$$

We can compute the integral of the non-conservative product under the above path:

$$\begin{aligned} \int_0^1 \mathbf{A}\left(\mathbf{W}\left(s;\mathbf{W}_L,\mathbf{W}_R\right)\right)\frac{\partial \mathbf{W}}{\partial s}\left(s;\mathbf{W}_L,\mathbf{W}_R\right)\mathrm{d}s &= \mathbf{F}^e(\mathbf{W}_R) - \mathbf{F}^e(\mathbf{W}_L) + \begin{pmatrix} 0 \\ 0 \\ \left(\frac{4}{3}\mu + K\right)\left([\![\rho]\!]\int_0^1 u(s)\mathrm{d}s - [\![\rho u]\!]\right) \end{pmatrix} \\ &= \mathbf{F}^e(\mathbf{W}_R) - \mathbf{F}^e(\mathbf{W}_L) + \begin{pmatrix} 0 \\ 0 \\ \left(\frac{4\mu}{3} + K\right)\widetilde{\rho}_{L,R}(u_L - u_R) \end{pmatrix}. \end{aligned} \tag{3.2}$$

Remark 3.1. *Noting that* $[\![\ln\rho]\!] = \frac{[\![\rho]\!]}{\widetilde{\rho}}$ *with a* $\widetilde{\rho} \in [\min\{\rho_L,\rho_R\},\max\{\rho_L,\rho_R\}]$, *we approximate the non-conservative product term* $\rho \mathrm{d}u$ *by* $\frac{\rho_L\rho_R}{\widetilde{\rho}}\left(u_R - u_L\right)$ *in* (3.2).

3.1.1. Elastic shock wave

We assume that $\mathbf{W}_L$ and $\mathbf{W}_R$ constitute an elastic shock wave, thereby satisfying the generalized Rankine-Hugoniot condition (2.13)

$$\varsigma\left(\mathbf{W}_R - \mathbf{W}_L\right) = \int_0^1 \mathbf{A}\left(\mathbf{W}\left(s;\mathbf{W}_L,\mathbf{W}_R\right)\right)\frac{\partial \mathbf{W}}{\partial s}\left(s;\mathbf{W}_L,\mathbf{W}_R\right)\mathrm{d}s. \tag{3.3}$$

Here, ς is the speed of the shock wave. The Lax's entropy condition in [32] requires that

$$\lambda_1^e(\mathbf{W}_L) \geq \varsigma \geq \lambda_1^e(\mathbf{W}_R) \quad \text{or} \quad \lambda_3^e(\mathbf{W}_L) \geq \varsigma \geq \lambda_3^e(\mathbf{W}_R). \tag{3.4}$$

We denote

$$\varphi = \sigma + \left(K + \frac{4}{3}\mu\right) \ln \rho.$$

Hooke's law states that φ is constant in the elastic solid [30,33,34]. For elastic rarefaction waves, Reference [33] proves that φ is precisely one of its Riemann invariants, which means that φ remains constant across the rarefaction wave. However, the reference does not rigorously prove that φ has the same property across elastic shock waves.

Theorem 3.1. *Let the two states $\mathbf{W}_L$ and $\mathbf{W}_R$ satisfy the generalized Rankine-Hugoniot condition (3.3) under the path (3.1) and the entropy condition (3.4), then $\varphi_L = \varphi_R$.*

Proof. If $[\![\rho]\!] = 0$, then $[\![u]\!] = [\![\sigma]\!] = 0$ and the conclusion holds clearly. We assume that $[\![\rho]\!] \neq 0$. The R-H relations are

$$\begin{aligned} [\![\rho u]\!] &= \varsigma[\![\rho]\!], \\ \left[\!\left[\rho u^2 - \sigma\right]\!\right] &= \varsigma[\![\rho u]\!], \\ [\![\rho u\sigma]\!] - \left(\frac{4}{3}\mu + K\right)\widetilde{\rho}_{L,R}[\![u]\!] &= \varsigma[\![\rho\sigma]\!]. \end{aligned}$$

Then we have

$$\begin{aligned} [\![\rho u\varphi]\!] &= [\![\rho u\sigma]\!] + \left(K + \frac{4}{3}\mu\right)[\![\rho u \ln \rho]\!] \\ &= \varsigma[\![\rho\sigma]\!] + \left(K + \frac{4}{3}\mu\right)\left([\![\rho u \ln \rho]\!] - \widetilde{\rho}_{L,R}[\![u]\!]\right) \\ &= \varsigma[\![\rho\sigma]\!] + \left(K + \frac{4}{3}\mu\right)([\![\rho u \ln \rho]\!] - (\{\{\rho u\}\} - \varsigma\{\{\rho\}\})[\![\ln \rho]\!]) \\ &= \varsigma[\![\rho\sigma]\!] + \left(K + \frac{4}{3}\mu\right)\varsigma[\![\rho \ln \rho]\!] \\ &= \varsigma[\![\rho\varphi]\!]. \end{aligned} \tag{3.5}$$

Combining the above equation with the first R-H relation, it holds that

$$(\{\{\rho u\}\} - \varsigma\{\{\rho\}\})[\![\varphi]\!] = 0,$$

Since

$$[\![\rho]\!](\{\{\rho u\}\} - \varsigma\{\{\rho\}\}) = [\![\rho]\!]\{\{\rho\}\}\{\{u\}\} - \frac{1}{4}[\![\rho]\!]^2[\![u]\!] - [\![\rho u]\!]\{\{\rho\}\} = -[\![u]\!]\left(\frac{1}{4}[\![\rho]\!]^2 + \{\{\rho\}\}^2\right),$$

it is enough to show that $[\![u]\!] \neq 0$. Otherwise, if $[\![u]\!] = 0$, then it follows that

$$\varsigma = [\![\rho u]\!]/[\![\rho]\!] = \{\{u\}\},$$

which contradicts the entropy condition. □

3.1.2. Elastic contact discontinuity

We then consider the contact discontinuity with the left-hand state $\mathbf{W}_L$ and right-hand state $\mathbf{W}_R$. A Riemann invariant is

$$\varsigma = u_L = u_R. \tag{3.6}$$

Theorem 3.2. *Let the two states $\mathbf{W}_L$ and $\mathbf{W}_R$ satisfy the generalized Rankine-Hugoniot condition (2.13) under the path (3.1) and the condition (3.6), then $\sigma_L = \sigma_R$.*

3.2. Riemann solver

Motivated by the Godunov method in [26], we construct the path for arbitrary two states $\mathbf{W}_L$ and $\mathbf{W}_R$ based on the solution of the Riemann problem:

$$\frac{\partial \mathbf{W}}{\partial t} + \mathbf{A}(\mathbf{W})\frac{\partial \mathbf{W}}{\partial x} = 0. \quad \mathbf{W}(x,0) = \begin{cases} \mathbf{W}_L, & x \leq 0 \\ \mathbf{W}_R, & x > 0 \end{cases}$$

The general structure of the Riemann solution is shown in Fig. 1. It has two nonlinear elastic waves, whose speeds are denoted by ς_L and ς_R respectively, and a contact discontinuity with the speed ς_*. The three elastic waves correspond to the three characteristic fields respectively, and divide the half-space into four constant regions. The two intermediate states are denoted by $\mathbf{W}_{*L} = \begin{pmatrix}\rho_{*L} & \rho_{*L}u_{*L} & \rho_{*L}\sigma_{x*L}\end{pmatrix}^{\mathrm{T}}$ and $\mathbf{W}_{*R} = \begin{pmatrix}\rho_{*R} & \rho_{*R}u_{*R} & \rho_{*R}\sigma_{x*R}\end{pmatrix}^{\mathrm{T}}$.

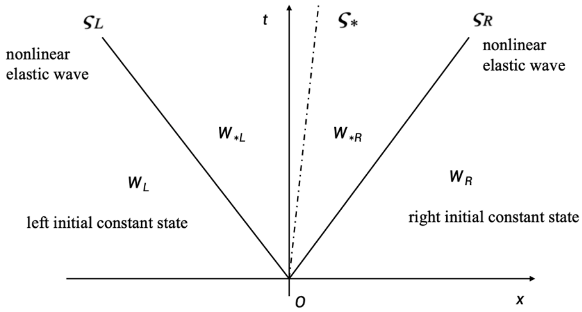

Fig. 1. Solution structure of Riemann problem for one-dimensional hypo-elastic solid.

Definition 3.1. *For every pair of elastic states $\mathbf{W}_L$ and $\mathbf{W}_R$, we suppose that a finite number $K \geq 1$ of speeds*

$$-\infty < \varsigma_1 < \varsigma_2 < \ldots < \varsigma_K < +\infty$$

and $m-1$ intermediate states

$$\mathbf{W}_0 = \mathbf{W}_L, \mathbf{W}_1, \ldots, \mathbf{W}_{K-1}, \mathbf{W}_K = \mathbf{W}_R.$$

in a continuous manner. For every arbitrary bounded set $\mathcal{O} \in \Omega$, there exists constant C_1 and C_2 such that

$$\begin{aligned}&|\mathbf{W}_k^1 - \mathbf{W}_L^1| \leq C_1 |\mathbf{W}_R^1 - \mathbf{W}_L^1|,\\ &|\mathbf{W}_k^1 - \mathbf{W}_k^2| \leq C_2\big(|\mathbf{W}_L^1 - \mathbf{W}_L^2| + |\mathbf{W}_R^1 - \mathbf{W}_R^2|\big),\ \forall 1 \leq k \leq K,\end{aligned}$$

for any $\mathbf{W}_L^1, \mathbf{W}_R^1, \mathbf{W}_L^2, \mathbf{W}_R^2 \in \mathcal{O}$. The function $\widetilde{\mathbf{V}} : \boldsymbol{R} \times \Omega \times \Omega \mapsto \Omega$ given by

$$\widetilde{\mathbf{V}}(v; \mathbf{W}_L, \mathbf{W}_R) = \mathbf{W}_k, \quad \text{if } \varsigma_k < v < \varsigma_{k+1}$$

is called an approximate Riemann solver.

In contrast to the Riemann solvers in [35], our approach does not explicitly impose the Rankine-Hugoniot conditions for the discontinuities. Instead, we use the path (3.1) to compute the non-conservative products across each discontinuity in the Riemann solver. Given two states $\mathbf{W}_L, \mathbf{W}_R$ and a Riemann solver, the path connecting these two states are the union of the paths of all discontinuities in the approximate Riemann solution. The linear path (3.1) is used for all discontinuities in the Riemann solution. Then the integral of non-conservative product is

$$\begin{aligned}\int_0^1 \mathbf{A}\big(\mathbf{W}(s; \mathbf{W}_L, \mathbf{W}_R)\big) \frac{\partial \mathbf{W}}{\partial s}(s; \mathbf{W}_L, \mathbf{W}_R)\mathrm{d}s &= \sum_{k=1}^{K} \int_0^1 \mathbf{A}\big(\mathbf{W}(s; \mathbf{W}_{k-1}, \mathbf{W}_k)\big) \frac{\partial \mathbf{W}}{\partial s}(s; \mathbf{W}_{k-1}, \mathbf{W}_k)\mathrm{d}s\\ &= \sum_{k=1}^{K} \mathbf{F}^e(\mathbf{W}_k) - \mathbf{F}^e(\mathbf{W}_{k-1}) + \begin{pmatrix}0 & 0 & \left(\frac{4\mu}{3} + K\right)\widetilde{\rho}_k\big(u_{k-1} - u_k\big)\end{pmatrix}^{\mathrm{T}},\\ &= \mathbf{F}^e(\mathbf{W}_R) - \mathbf{F}^e(\mathbf{W}_L) + \begin{pmatrix}0 & 0 & \left(\frac{4\mu}{3} + K\right)\sum_{k=1}^{K}\widetilde{\rho}_k\big(u_{k-1} - u_k\big)\end{pmatrix}^{\mathrm{T}},\end{aligned}$$

where

$$\widetilde{\rho}_k = \begin{cases}\rho_{k-1}\rho_k \frac{\ln\rho_k - \ln\rho_{k-1}}{\rho_k - \rho_{k-1}}, & \rho_{k-1} \neq \rho_k\\ \rho_k, & \rho_{k-1} = \rho_k\end{cases} \tag{3.7}$$

The path based on an Riemann solver is a piecewise smooth and continuous mapping. The definition of the Riemann solver ensures that it satisfies the requirements of the path definition. Some existing approximate Riemann solvers can be applied in this framework. We give two alternative Riemann solvers below.

3.2.1. HLLC solver

The HLLC (Harten-Lax-van Leer Contact) method prespecifies the wave speeds in the Riemann solution based on the eigenvalues. We assume that the speeds of the left-going and right-going waves are

$$\varsigma_1 = \min\big(u_L - c_L^e, u_R - c_R^e\big), \quad \varsigma_3 = \max\big(u_L + c_L^e, u_R + c_R^e\big), \tag{3.8}$$

where c_L^e and c_R^e are specific sound speeds. By the R-H relation, one can obtain the intermediate states:

$$\begin{aligned}
&\varsigma_2 = u_1,\\
&\sigma_1 = \sigma_2 = \sigma_L - \rho_L(\varsigma_1 - u_L)(u_1 - u_L),\\
&u_1 = u_2 = \frac{\sigma_L - \sigma_R + \rho_L u_L(\varsigma_1 - u_L) - \rho_R u_R(\varsigma_3 - u_R)}{\rho_L(\varsigma_1 - u_L) - \rho_R(\varsigma_3 - u_R)},\\
&\rho_1 = \frac{\rho_L(u_L - \varsigma_1)}{u_1 - \varsigma_1}, \rho_2 = \frac{\rho_R(u_R - \varsigma_3)}{u_2 - \varsigma_3}.
\end{aligned}$$

Note that in the HLLC solver, every discontinuity satisfies the R-H conditions, and therefore

$$\int_0^1 \mathbf{A}(\mathbf{W}(s;\mathbf{W}_L,\mathbf{W}_R))\frac{\partial \mathbf{W}}{\partial s}(s;\mathbf{W}_L,\mathbf{W}_R)\mathrm{d}s = \sum_{k=1}^{3}\varsigma_k(\mathbf{W}_k - \mathbf{W}_{k-1}).$$

Clearly, the HLLC solver satisfies the definition of a Riemann solver if we assume that $\rho_L \geq \underline{\rho}, \rho_R \geq \underline{\rho}$ for some bound $\underline{\rho} > 0$.

3.2.2. Linearized shock Riemann solver (LSRS)

In this section, we present another approximate Riemann solver, whose underlying idea is to approximate each nonlinear wave in the Riemann solution with a linearized shock wave. Such an idea has been used in [29,36]. By the R-H relations, the exact intermediate states satisfy

$$u_1 = u_L + \sqrt{(\sigma_L - \sigma_1)\left(\frac{1}{\rho_L} - \frac{1}{\rho_1}\right)}, \quad u_2 = u_R - \sqrt{(\sigma_R - \sigma_2)\left(\frac{1}{\rho_R} - \frac{1}{\rho_2}\right)}. \tag{3.9}$$

According to Theorem 3.1, we have

$$\rho_1 = \rho_L \exp\left(\frac{3\sigma_L - 3\sigma_1}{4\mu + 3K}\right), \quad \rho_2 = \rho_R \exp\left(\frac{3\sigma_R - 3\sigma_2}{4\mu + 3K}\right). \tag{3.10}$$

Expanding the exponential function in (3.10) as a Taylor series around σ_1/σ_L or σ_2/σ_R near 1 (i.e., $|\sigma_1/\sigma_L - 1| < 1$ or $|\sigma_2/\sigma_R - 1| < 1$), we have

$$\rho_1 = \rho_L\left(1 + \frac{3\sigma_L - 3\sigma_1}{4\mu + 3K} + \mathcal{O}\left(\frac{3\sigma_L - 3\sigma_1}{4\mu + 3K}\right)^2\right), \quad \rho_2 = \rho_R\left(1 + \frac{3\sigma_R - 3\sigma_2}{4\mu + 3K} + \mathcal{O}\left(\frac{3\sigma_R - 3\sigma_2}{4\mu + 3K}\right)^2\right), \tag{3.11}$$

Substitute (3.11) into (3.10) to obtain

$$\sqrt{(\sigma_L - \sigma_1)\left(\frac{1}{\rho_L} - \frac{1}{\rho_1}\right)} = -\frac{\sigma_L}{c_L^e\rho_L}\left(\frac{\sigma_1}{\sigma_L} - 1\right) + \mathcal{O}\left(\frac{\sigma_1}{\sigma_L} - 1\right)^2, c_L^e = \sqrt{\frac{4\mu + 3K}{3\rho_L}}, \tag{3.12}$$

$$\sqrt{(\sigma_R - \sigma_2)\left(\frac{1}{\rho_R} - \frac{1}{\rho_2}\right)} = -\frac{\sigma_R}{c_R^e\rho_R}\left(\frac{\sigma_2}{\sigma_R} - 1\right) + \mathcal{O}\left(\frac{\sigma_2}{\sigma_R} - 1\right)^2, c_R^e = \sqrt{\frac{4\mu + 3K}{3\rho_R}}. \tag{3.13}$$

Taking the leading term of (3.12) and (3.13), we have

$$\sqrt{(\sigma_L - \sigma_1)\left(\frac{1}{\rho_L} - \frac{1}{\rho_1}\right)} \approx -\frac{\sigma_L}{c_L^e\rho_L}\left(\frac{\sigma_1}{\sigma_L} - 1\right), \tag{3.14}$$

$$\sqrt{(\sigma_R - \sigma_2)\left(\frac{1}{\rho_R} - \frac{1}{\rho_2}\right)} \approx -\frac{\sigma_R}{c_R^e\rho_R}\left(\frac{\sigma_2}{\sigma_R} - 1\right). \tag{3.15}$$

Substituting (3.14) and (3.15) into (3.9), one can get

$$\sigma_1 = \sigma_2 = \frac{1}{\frac{1}{c_R^e\rho_R} + \frac{1}{c_L^e\rho_L}}\left(\frac{\sigma_R}{c_R^e\rho_R} + \frac{\sigma_L}{c_L^e\rho_L}\right) + u_R - u_L. \tag{3.16}$$

Substituting (3.14)-(3.16) into (3.9) , we can obtain

$$u_1 = u_2 = \frac{1}{2}(u_L + u_R) + \frac{1}{2}\left[\frac{\sigma_L}{c_L^e\rho_L}\left(\frac{\sigma_1}{\sigma_L} - 1\right) - \frac{\sigma_R}{c_R^e\rho_R}\left(\frac{\sigma_2}{\sigma_R} - 1\right)\right]. \tag{3.17}$$

In summary, we can obtain the intermediate states:

$$\sigma_1=\sigma_2=\frac{1}{\frac{1}{c_R^e\rho_R}+\frac{1}{c_L^e\rho_L}}\left(\frac{\sigma_R}{c_R^e\rho_R}+\frac{\sigma_L}{c_L^e\rho_L}\right)+u_R-u_L,$$

$$u_1=u_2=\frac{1}{2}\left(u_L+u_R\right)+\frac{1}{2}\left[\frac{\sigma_L}{c_L^e\rho_L}\left(\frac{\sigma_1}{\sigma_L}-1\right)-\frac{\sigma_R}{c_R^e\rho_R}\left(\frac{\sigma_2}{\sigma_R}-1\right)\right],$$

$$\rho_1=\rho_L\exp\left(\frac{3\sigma_L-3\sigma_1}{4\mu+3K}\right),$$

$$\rho_2=\rho_R\exp\left(\frac{3\sigma_R-3\sigma_2}{4\mu+3K}\right),$$

$$\varsigma_1=\begin{cases}(\rho_1u_1-\rho_Lu_L)/(\rho_1-\rho_L), & \rho_L\neq\rho_1\\ u_L-c_L^e, & \rho_L=\rho_1\end{cases},$$

$$\varsigma_2=u_1,$$

$$\varsigma_3=\begin{cases}(\rho_2u_2-\rho_Ru_R)/(\rho_2-\rho_R), & \rho_R\neq\rho_2\\ u_R+c_R^e, & \rho_R=\rho_2\end{cases}.$$

Similarly, if we assume the uniform bound

$$\rho_L\geq\underline{\rho}>0,\ \rho_R\geq\underline{\rho}>0,$$

it is straightforward to demonstrate that this solver satisfies the definition of a Riemann solver.

4. Path-conservative scheme

4.1. Path-conservative scheme for hypo-elastic solid

In this section, we present the path-conservative scheme for the Cauchy problem of the hypo-elastic solid model

$$\begin{cases}\dfrac{\partial\mathbf{W}}{\partial t}+\dfrac{\partial\mathbf{F}^e(\mathbf{W})}{\partial x}=\mathbf{S}(\mathbf{W}),\\ \mathbf{W}(x,0)=\mathbf{W}_0(x),\ x\in[a,b],\ t\in[0,T].\end{cases}$$

The finite computational domain $[a,b]$ is divided into N non-overlapping cells:

$$a=x_{1/2}<\ldots<x_{i-1/2}<x_{i+1/2}<\ldots<x_{M+1/2}=b.$$

We assume that the mesh is regular, i.e. $|x_{i+1/2}-x_{i-1/2}|\equiv h$. In the time direction, we also use the regular division:

$$t^n=n\Delta t,\ \Delta t \text{ is a constant.}$$

We denote by $\mathbf{W}_i^n$ the average value of the numerical solution on the cell $\left[x_{i-1/2},x_{i+1/2}\right]$ and at the time step t^n. The initial data for the finite volume scheme is obtained by a projection operator

$$\mathbf{W}_i^0=\frac{1}{h}\int_{x_{i-1/2}}^{x_{i+1/2}}\mathbf{W}_0(x)\mathrm{d}x.$$

The numerical solution is

$$\mathbf{W}_h(x,t)=1_{[x_{i-1/2},x_{i+1/2})\times[t^n,t^{n+1})}\mathbf{W}_i^n.$$

The constraint for the time step size is

$$\Delta t=\frac{CFL\cdot\Delta x}{\max_{1\leq k\leq 3}|\lambda_k^e(\mathbf{W}_h)|},\ CFL\leq\frac{1}{2}.$$

The path-conservative finite volume scheme is

$$\mathbf{W}_i^{n+1}=\mathbf{W}_i^n-\frac{\Delta t}{h}\left(\mathbf{D}_{i-1/2}^{+}+\mathbf{D}_{i+1/2}^{-}\right), \tag{4.1}$$

where $D_{i-1/2}^{\pm}$ are the numerical fluxes that satisfy

$$\mathbf{D}_{i+1/2}^{-}+\mathbf{D}_{i+1/2}^{+}=\int_0^1\mathbf{A}\big(\Phi\big(s;\mathbf{W}_i,\mathbf{W}_{i+1}\big)\big)\frac{\partial\Phi}{\partial s}\big(s;\mathbf{W}_i,\mathbf{W}_{i+1}\big)\mathrm{d}s. \tag{4.2}$$

In this paper, a Godunov-type method is used to compute the numerical fluxes. In the cell interface $x_{i+1/2}$, we consider the Riemann problem

$$\begin{cases}\dfrac{\partial\mathbf{W}}{\partial t}+\mathbf{A}(\mathbf{W})\dfrac{\partial\mathbf{W}}{\partial x}=0,\\ \mathbf{W}(x,0)=\begin{cases}\mathbf{W}_i^n, & x\leq 0,\\ \mathbf{W}_{i+1}^n, & x>0,\end{cases}\end{cases} \tag{4.3}$$

and denote the approximate Riemann solution by $\widetilde{\mathbf{V}}(v;\mathbf{W}_L,\mathbf{W}_R)$. The numerical fluxes are

$$\mathbf{D}^-_{i+1/2}=\int_0^1 \mathbf{A}\Big(\Phi\Big(s;\mathbf{W}_i^n,\widetilde{\mathbf{V}}(0;\mathbf{W}_i^n,\mathbf{W}_{i+1}^n)\Big)\Big)\frac{\partial\Phi}{\partial s}\Big(s;\mathbf{W}_i^n,\widetilde{\mathbf{V}}(0;\mathbf{W}_i^n,\mathbf{W}_{i+1}^n)\Big)\mathrm{d}s,$$

$$\mathbf{D}^+_{i+1/2}=\int_0^1 \mathbf{A}\Big(\Phi\Big(s;\widetilde{\mathbf{V}}(0;\mathbf{W}_i^n,\mathbf{W}_{i+1}^n),\mathbf{W}_{i+1}^n\Big)\Big)\frac{\partial\Phi}{\partial s}\Big(s;\widetilde{\mathbf{V}}(0;\mathbf{W}_i^n,\mathbf{W}_{i+1}^n),\mathbf{W}_{i+1}^n\Big)\mathrm{d}s.$$

Substituting the paths into the numerical fluxes, we have

$$\mathbf{D}^-_{i+1/2}=\sum_{k=1}^{K}\min(\varsigma_k,0)\left(\mathbf{F}^e(\mathbf{W}_{k+1})-\mathbf{F}^e(\mathbf{W}_k)+\left(\frac{4\mu}{3}+K\right)\widetilde{\rho}_k\begin{pmatrix}0\\0\\u_{k-1}-u_k\end{pmatrix}\right),$$

$$\mathbf{D}^+_{i+1/2}=\sum_{k=1}^{K}\max(\varsigma_k,0)\left(\mathbf{F}^e(\mathbf{W}_{k+1})-\mathbf{F}^e(\mathbf{W}_k)+\left(\frac{4\mu}{3}+K\right)\widetilde{\rho}_k\begin{pmatrix}0\\0\\u_{k-1}-u_k\end{pmatrix}\right),$$

where the intermediate states $W_k(1\le k\le K)$ and wave speeds $\varsigma_k(1\le k\le K)$ are given by a Riemann solver, and $\widetilde{\rho}_k$ are given by (3.7).

4.2. Path-conservative scheme for hypo-elastic plastic solid

4.2.1. Supplement to the scheme for hypo-elastic solid

The elastic and plastic states of a solid are determined based on the deviatoric stress s. However, there is no governing equation for s in the perfect hypo-elastic model, we add an evolution equation of s in the path-conservative finite volume scheme. According to Hooke's law, we have

$$\frac{\partial(\rho s)}{\partial t}+\frac{\partial(\rho u s)}{\partial x}=\frac{4}{3}\mu\rho\frac{\partial u}{\partial x}.$$

Thus, the governing equations for an elastic-plastic solid in the elastic state can be rewritten as

$$\frac{\partial\overline{\mathbf{W}}}{\partial t}+\frac{\partial\overline{\mathbf{F}}^e(\overline{\mathbf{W}})}{\partial x}=\overline{\mathbf{S}}(\overline{\mathbf{W}}),$$

$$\overline{\mathbf{W}}=\begin{pmatrix}\rho\\\rho u\\\rho\sigma\\s\end{pmatrix},\quad \overline{\mathbf{F}}^e(\overline{\mathbf{W}})=\begin{pmatrix}\rho u\\\rho u^2-\sigma\\\rho u\sigma\\\rho u s\end{pmatrix},\quad \overline{\mathbf{S}}(\overline{\mathbf{W}})=\begin{pmatrix}0\\0\\\left(K+\frac{4}{3}\mu\right)\rho\frac{\partial u}{\partial x}\\\frac{4}{3}\mu\rho\frac{\partial u}{\partial x}\end{pmatrix}. \tag{4.4}$$

The discretization of the non-conservative terms in the augmented equation is identical to that in the hypo-elastic equation. The path-conservative scheme for the equation above is

$$\overline{\mathbf{W}}_i^{n+1}=\overline{\mathbf{W}}_i^{n}-\frac{\Delta t}{h}\left(\overline{\mathbf{D}}^{n,+}_{i-1/2}+\overline{\mathbf{D}}^{n,-}_{i+1/2}\right), \tag{4.5}$$

$$\overline{\mathbf{D}}^-_{i+1/2}=\sum_{k=1}^{K}\min(\varsigma_k,0)\left(\overline{\mathbf{F}}^e(\mathbf{W}_{k+1})-\overline{\mathbf{F}}^e(\mathbf{W}_k)+\widetilde{\rho}_k\begin{pmatrix}0\\0\\\left(\frac{4\mu}{3}+K\right)(u_{k-1}-u_k)\\\frac{4\mu}{3}(u_{k-1}-u_k)\end{pmatrix}\right),$$

$$\overline{\mathbf{D}}^+_{i+1/2}=\sum_{k=1}^{K}\max(\varsigma_k,0)\left(\overline{\mathbf{F}}^e(\mathbf{W}_{k+1})-\overline{\mathbf{F}}^e(\mathbf{W}_k)+\widetilde{\rho}_k\begin{pmatrix}0\\0\\\left(\frac{4\mu}{3}+K\right)(u_{k-1}-u_k)\\\frac{4\mu}{3}(u_{k-1}-u_k)\end{pmatrix}\right).$$

4.2.2. Supplement to the scheme for plastic solid

The governing equations for the solid in plastic state take the form of a hyperbolic conservation law (2.8), allowing us to employ classical conservative schemes. Within the Eulerian formulation, convection can induce a transition from a plastic state to an elastic state in a fixed computational cell [37]. To account for this, we add the transport equation for the deviatoric stress:

$$\frac{\partial(\rho s)}{\partial t}+\frac{\partial(\rho u s)}{\partial x}=0. \tag{4.6}$$

For cells that remain in the plastic state throughout, s is constant, and thus the above equation is always satisfied. We discretize the equation

$$\frac{\partial\overline{\mathbf{U}}}{\partial t}+\frac{\partial\overline{\mathbf{F}}^p(\overline{\mathbf{U}})}{\partial x}=0,\quad \overline{\mathbf{U}}=\begin{pmatrix}\rho\\\rho u\\E\\\rho s\end{pmatrix},\ \overline{\mathbf{F}}^p(\overline{\mathbf{U}})=\begin{pmatrix}\rho u\\\rho u^2-\sigma\\(E-\sigma)u\\\rho u s\end{pmatrix} \tag{4.7}$$

by a conservative finite volume scheme

$$\overline{\mathbf{U}}_i^{n+1} = \overline{\mathbf{U}}_i^n - \frac{\Delta t}{h}\left(\overline{\mathbf{F}}\left(\overline{\mathbf{U}}_{i+1/2}^{n+1/2}\right) - \overline{\mathbf{F}}\left(\overline{\mathbf{U}}_{i-1/2}^{n+1/2}\right)\right), \tag{4.8}$$

Here $\overline{\mathbf{U}}_{i+1/2}^{n+1/2}$ is the state at the t-axis in the Riemann solution with the left initial data $\overline{\mathbf{U}}_i^n$ and right initial data $\overline{\mathbf{U}}_{i+1}^n$. We use the HLLC solver for the Eqs. (4.7):

$$\begin{aligned}
&\varsigma_1 = \min\left(u_L - c_L^p, u_R - c_R^p\right),\\
&\varsigma_2 = u_1,\\
&\varsigma_3 = \max\left(u_L + c_L^p, u_R + c_R^p\right),\\
&\sigma_1 = \sigma_2 = \sigma_L - \rho_L\left(\varsigma_1 - u_L\right)\left(u_1 - u_L\right),\\
&u_1 = u_2 = \frac{\sigma_L - \sigma_R + \rho_L u_L\left(\varsigma_1 - u_L\right) - \rho_R u_R\left(\varsigma_3 - u_R\right)}{\rho_L\left(\varsigma_1 - u_L\right) - \rho_R\left(\varsigma_2 - u_R\right)},
\end{aligned}
\qquad
\begin{aligned}
&\rho_1 = \frac{\rho_L\left(u_L - \varsigma_1\right)}{u_1 - \varsigma_1},\\
&\rho_2 = \frac{\rho_R\left(u_R - \varsigma_2\right)}{u_2 - \varsigma_2},\\
&s_1 = s_L,\\
&s_2 = s_R,\\
&E_1 = E_L + (\varsigma_2 - u_L)(\varsigma_2 + \sigma_1/(\rho_L(\varsigma_1 - u_L))),\\
&E_2 = E_R + (\varsigma_2 - u_R)(\varsigma_2 + \sigma_2/(\rho_R(\varsigma_3 - u_R))).
\end{aligned}$$

Remark 4.1. *It is noteworthy to highlight the differences in the evolution equations for s between the two models. In practice, when an elastic shock wave enters a plastic cell, the Eq. (4.6) should be modified. However, to maintain algorithmic simplicity, we neglect this error, as that cell will be identified as being in the elastic state at the next time step, and s will subsequently evolve according to Hooke's law.*

4.2.3. The transition between elastic and plastic states

If the solid is in an elastic state, then we use a path-conservative finite volume scheme (4.5) for the evolution of variables. If the solid changes from an elastic state to a plastic state, then we use the conservative finite volume scheme (4.8). The transition between elastic and plastic states is mediated by pressure. Assume that the cell I_i is in an elastic state at the time step t^n, and it changes to a plastic state at the next time step t^{n+1}, which means

$$\left|s_i^n\right| < \frac{2}{3}Y_0, \ \left|s_i^{n+1}\right| \geq \frac{2}{3}Y_0.$$

We then get the plastic variables at the time step t^{n+1} by

$$\begin{aligned}
&\rho_i^{n+1} s_i^{n+1} = \pm\frac{2}{3}Y_0 \rho_i^{n+1},\\
&E_i^{n+1} = \frac{s_i^{n+1} - \sigma_i^{n+1} - c_0^2(\rho_i^{n+1} - \rho_0)}{\gamma - 1} + \frac{1}{2}\rho_i^{n+1}(u_i^{n+1})^2.
\end{aligned}$$

On the other hand, if the cell I_i is in a plastic state at the time step t^n and changes to an elastic state at the time step t^{n+1}, i.e.

$$\left|s_i^n\right| \geq \frac{2}{3}Y_0, \ \left|s_i^{n+1}\right| < \frac{2}{3}Y_0,$$

then we assign the values

$$\rho_i^{n+1}\sigma_i^{n+1} = \rho_i^{n+1}\left(-c_0^2(\rho_i^{n+1} - \rho_0) - (\gamma - 1)(E_i^{n+1} - \rho_i^{n+1}(u_i^{n+1})^2/2) + s_i^{n+1}\right).$$

4.2.4. Numerical flux for elastic-plastic interface

In this section, we present the numerical flux at the interface between elastic and plastic cells. Without loss of generality, we assume that at time t^n, the cell I_i is in an elastic state and the cell I_{i+1} is in a plastic state. To determine the flux at the interface $x_{i+1/2}$, it is sufficient to specify the states at the t-axis's $\overline{\mathbf{W}}_{i+1/2}^{n+1/2}$ and $\overline{\mathbf{U}}_{i+1/2}^{n+1/2}$,

Firstly, we solve the elastic-plastic Riemann problem. The structure of the Riemann solution is illustrated in the Fig. 2, where four constant regions are separated by an elastic nonlinear wave, a plastic nonlinear wave, and a contact discontinuity.

Remark 4.2. *Different studies handle the elastic-plastic transition in Riemann solvers differently. Some consider introducing an elastic limit state to connect elastic and plastic states, thereby making the wave structure more complex [38,39]. Others do not introduce this limit; achieving numerical fluxes more simply [40,41]. In this paper, we choose not to introduce the limit state to maintain a simpler wave structure.*

Across the contact discontinuity, both the velocity and the deviatoric stress remain continuous:

$$u_1 = u_2, \sigma_1 = \sigma_2.$$

Similar to the previous discussion, we can employ an approximate Riemann solver. The approximate solutions for the two methods introduced above are as follows:

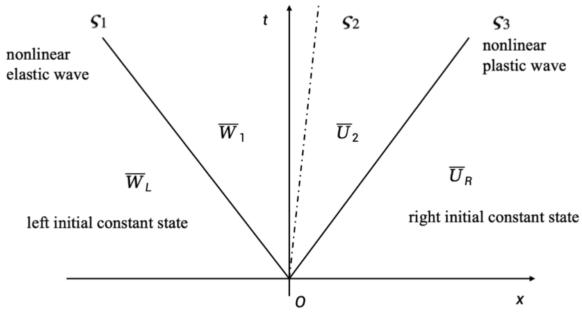

Fig. 2. Solution structure of one-dimensional elastic-plastic Riemann problem.

- HLLC solver:

$$\begin{aligned}
&\varsigma_1 = \min\left(u_L - c_L^e, u_R - c_R^p\right),\\
&\varsigma_2 = u_1,\\
&\varsigma_3 = \max\left(u_L + c_L^e, u_R + c_R^p\right),\\
&\sigma_1 = \sigma_L - \rho_L\left(\varsigma_1 - u_L\right)\left(u_1 - u_L\right),\\
&u_1 = u_2 = \frac{\sigma_L - \sigma_R + \rho_L u_L\left(\varsigma_1 - u_L\right) - \rho_R u_R\left(\varsigma_3 - u_R\right)}{\rho_L\left(\varsigma_1 - u_L\right) - \rho_R\left(\varsigma_2 - u_R\right)},
\end{aligned}$$

$$\begin{aligned}
&\rho_1 = \frac{\rho_L\left(u_L - \varsigma_1\right)}{u_1 - \varsigma_1},\\
&\rho_2 = \frac{\rho_R\left(u_R - \varsigma_3\right)}{u_2 - \varsigma_3},\\
&s_1 = \frac{4\mu}{3}\ln\frac{\rho_1}{\rho_L} + s_L,\\
&s_2 = s_R,\\
&E_2 = E_R + (\varsigma_2 - u_R)(\varsigma_2 + \sigma_2/(\rho_R(\varsigma_3 - u_R))).
\end{aligned}$$

- LSRS method:

$$\begin{aligned}
&\varsigma_1 = \begin{cases}(\rho_1 u_1 - \rho_L u_L)/(\rho_1 - \rho_L), & \rho_L \neq \rho_1\\ u_L - c_L^e, & \rho_L = \rho_1\end{cases},\\
&\varsigma_2 = u_1,\\
&\varsigma_3 = \begin{cases}(\rho_2 u_2 - \rho_R u_R)/(\rho_2 - \rho_R), & \rho_R \neq \rho_2\\ u_R + c_R^e, & \rho_R = \rho_2\end{cases},\\
&\sigma_1 = \frac{1}{\frac{1}{c_R^e\rho_R} + \frac{1}{c_L^e\rho_L}}\left(\frac{\sigma_R}{c_R^e\rho_R} + \frac{\sigma_L}{c_L^e\rho_L}\right) + u_R - u_L,\\
&u_1 = u_2 = \frac{1}{2}\left(u_L + u_R\right) + \frac{1}{2}\left[\frac{\sigma_L}{c_L^e\rho_L}\left(\frac{\sigma_1}{\sigma_L} - 1\right) - \frac{\sigma_R}{c_R^e\rho_R}\left(\frac{\sigma_1}{\sigma_R} - 1\right)\right],
\end{aligned}$$

$$\begin{aligned}
&\rho_1 = \rho_L \exp\left(\frac{3\sigma_L - 3\sigma_1}{4\mu + 3K}\right),\\
&\rho_2 = \rho_R \exp\left(\frac{3\sigma_R - 3\sigma_1}{4\mu + 3K}\right),\\
&s_1 = \frac{4\mu}{3}\ln\frac{\rho_1}{\rho_L} + s_L,\\
&s_2 = s_R,\\
&E_2 = E_R + (\varsigma_2 - u_R)(\varsigma_2 + \sigma_2/(\rho_R(\varsigma_3 - u_R))).
\end{aligned}$$

Secondly, we need to account for the elastic-plastic state transition in the approximate Riemann solution. The elastic-plastic transition in the numerical flux should align with the elastic-plastic transition in the numerical solution, so we use

$$\begin{aligned}
E_L &= \frac{s_L - \sigma_L - c_0^2(\rho_L - \rho_0)}{\gamma - 1} + \frac{1}{2}\rho_L(u_L)^2,\\
E_1 &= \frac{s_1 - \sigma_1 - c_0^2(\rho_1 - \rho_0)}{\gamma - 1} + \frac{1}{2}\rho_1(u_1)^2,\\
\sigma_2 &= -c_0^2(\rho_2 - \rho_0) - (\gamma - 1)\left(E_2 - \frac{\rho_2(u_2)^2}{2}\right) + s_2,\\
\sigma_R &= -c_0^2(\rho_R - \rho_0) - (\gamma - 1)\left(E_R - \frac{\rho_R(u_R)^2}{2}\right) + s_R.
\end{aligned} \tag{4.9}$$

5. Two-dimensional extension

5.1. Governing equations

Reference [42] indicates that Hooke's law, pertaining to the hydrostatic pressure p in the governing equation, can alternatively be substituted with the energy conservation equation and the equation of state. This approach still results in a hypo-elastic model. In extreme environments, such as inertial confinement fusion, solids are subjected to high temperatures and pressures, exhibiting characteristics of compressible fluids, where Hooke's law no longer applies [43–45]. Therefore, we consider extending the one-dimensional method presented in this paper to these situations, broadening the proposed method's application scenarios. Consequently, we adopt the governing equations of two-dimensional hypo-elastic plastic solids in [10,37,45].

$$
\begin{aligned}
&\frac{\partial \rho}{\partial t}+\frac{\partial(\rho u)}{\partial x}+\frac{\partial(\rho v)}{\partial y}=0,\\
&\frac{\partial(\rho u)}{\partial t}+\frac{\partial\left(\rho u^2+p-s_{xx}\right)}{\partial x}+\frac{\partial\left(\rho u v-s_{xy}\right)}{\partial y}=0,\\
&\frac{\partial(\rho v)}{\partial t}+\frac{\partial\left(\rho u v-s_{xy}\right)}{\partial x}+\frac{\partial\left(\rho v^2+p-s_{yy}\right)}{\partial y}=0,\\
&\frac{\partial E}{\partial t}+\frac{\partial\left(uE+\left(p-s_{xx}\right)u-s_{xy}v\right)}{\partial x}+\frac{\partial\left(vE+\left(p-s_{yy}\right)v-s_{xy}u\right)}{\partial y}=0.
\end{aligned}
$$

Here, the variables are the density ρ, the x-directional velocity u,the y-directional velocity v, the total energy per unit volume $E=\rho e+\frac{1}{2}\rho(u^2+v^2)$ with e representing the specific internal energy. s_{xy} is the shear stress. s_{xx} and s_{yy} are the x- and y-directional deviatoric stresses, respectively. The total stress decomposition is

$$
\sigma_{xx}=-p+s_{xx},\ \sigma_{yy}=-p+s_{yy},
$$

where σ_{xx} is the x-directional total stress, and σ_{yy} is the y-directional total stress. The hydrostatic pressure p satisfies the stiffened-gas equation of state

$$
p=c_0^2(\rho-\rho_0)+(\gamma-1)\rho e.
$$

The constitutive model is divided into an elastic phase and a plastic phase. Elastic solids satisfy the von Mises yield condition:

$$
s_{xx}^2+s_{yy}^2+2s_{xy}^2+(s_{xx}+s_{yy})^2\le\frac{2}{3}(Y_0)^2.
$$

In the hypo-elastic solid model, the deviatoric stresses satisfy the differential stress-strain relationships

$$
\dot{s}_{xx}=2\mu(\dot{\epsilon}_x+\frac{1}{3}\frac{\dot{\rho}}{\rho}),\dot{s}_{yy}=2\mu(\dot{\epsilon}_y+\frac{1}{3}\frac{\dot{\rho}}{\rho}),\ \dot{s}_{xy}=\mu\dot{\epsilon}_{xy}.
$$

μ is the shear modulus. The superscript "." denotes the material derivative. $\dot{s}_{xx}$ and $\dot{s}_{yy}$ are the deviator stress rates, $\dot{s}_{xy}$ is the shear stress rate, and $\dot{\rho}$ is the density rate. The strain rates are

$$
\dot{\epsilon}_x=\frac{\partial u}{\partial x},\ \dot{\epsilon}_y=\frac{\partial v}{\partial y},\ \dot{\epsilon}_{xy}=\frac{\partial v}{\partial x}+\frac{\partial u}{\partial y}.
$$

So the equations of deviator stress and shear stress can be rewritten as

$$
\begin{aligned}
&\frac{\partial(\rho s_{xx})}{\partial t}+\frac{\partial(\rho u s_{xx})}{\partial x}+\frac{\partial(\rho v s_{xx})}{\partial y}-\frac{2}{3}\mu\rho\left(2\frac{\partial u}{\partial x}-\frac{\partial v}{\partial y}\right)=0,\\
&\frac{\partial(\rho s_{yy})}{\partial t}+\frac{\partial(\rho u s_{yy})}{\partial x}+\frac{\partial(\rho v s_{yy})}{\partial y}-\frac{2}{3}\mu\rho\left(2\frac{\partial v}{\partial y}-\frac{\partial u}{\partial x}\right)=0,\\
&\frac{\partial(\rho s_{xy})}{\partial t}+\frac{\partial(\rho u s_{xy})}{\partial x}+\frac{\partial(\rho v s_{xy})}{\partial y}-\mu\rho\left(\frac{\partial v}{\partial x}+\frac{\partial u}{\partial y}\right)=0.
\end{aligned}
$$

Let

$$
\begin{aligned}
\mathbf{W}&=\begin{pmatrix}\rho & \rho u & \rho v & E & \rho s_{xx} & \rho s_{yy} & \rho s_{xy}\end{pmatrix}^{\mathrm{T}},\\
\mathbf{F}=\mathbf{F}(W)&=\begin{pmatrix}\rho u & \rho u^2+p-s_{xx} & \rho uv-s_{xy} & uE+(p-s_{xx})u-s_{xy}v & \rho u s_{xx} & \rho u s_{yy} & \rho u s_{xy}\end{pmatrix}^{\mathrm{T}},\\
\mathbf{G}=\mathbf{G}(W)&=\begin{pmatrix}\rho v & \rho uv-s_{xy} & \rho v^2+p-s_{yy} & vE+(p-s_{yy})v-s_{xy}u & \rho v s_{xx} & \rho v s_{yy} & \rho v s_{xy}\end{pmatrix}^{\mathrm{T}}.
\end{aligned}
$$

The two-dimensional governing equations for the hypo-elastic solid are

$$
\frac{\partial\mathbf{W}}{\partial t}+\mathbf{A}(\mathbf{W})\frac{\partial\mathbf{W}}{\partial x}+\mathbf{B}(\mathbf{W})\frac{\partial\mathbf{W}}{\partial y}=0, \tag{5.1}
$$

$$
\mathbf{A}(\mathbf{W})=\frac{\partial\mathbf{F}(\mathbf{W})}{\partial\mathbf{W}}+\left(\begin{array}{ccccccc}
\multicolumn{7}{c}{0_{4\times7}}\\
\frac{4\mu u}{3} & -\frac{4\mu}{3} & 0 & 0 & 0 & 0 & 0\\
-\frac{2\mu u}{3} & \frac{2\mu}{3} & 0 & 0 & 0 & 0 & 0\\
\mu v & 0 & -\mu & 0 & 0 & 0 & 0
\end{array}\right),
$$

$$
\mathbf{B}(\mathbf{W})=\frac{\partial\mathbf{G}(\mathbf{W})}{\partial\mathbf{W}}+\left(\begin{array}{ccccccc}
\multicolumn{7}{c}{0_{4\times7}}\\
-\frac{2\mu v}{3} & 0 & \frac{2\mu}{3} & 0 & 0 & 0 & 0\\
\frac{4\mu v}{3} & 0 & -\frac{4\mu}{3} & 0 & 0 & 0 & 0\\
\mu u & -\mu & 0 & 0 & 0 & 0 & 0
\end{array}\right).
$$

The eigenvalues of the matrix $\mathbf{A}(\mathbf{W})$ are

$$
\lambda_1(\mathbf{A})=u-c_x^e,\lambda_2(\mathbf{A})=u-c^s,\lambda_3(\mathbf{A})=\lambda_4(\mathbf{A})=\lambda_5(\mathbf{A})=u,\lambda_6(\mathbf{A})=u+c^s,\lambda_7(\mathbf{A})=u+c_x^e. \tag{5.2}
$$

The eigenvalues of the matrix $\mathbf{B}(\mathbf{W})$ are

$$\lambda_1(\mathbf{B}) = v - c_y^e, \lambda_2(\mathbf{B}) = v - c^s, \lambda_3(\mathbf{B}) = \lambda_4(\mathbf{B}) = \lambda_5(\mathbf{B}) = v, \lambda_6(\mathbf{B}) = v + c^s, \lambda_7(\mathbf{B}) = v + c_y^e. \tag{5.3}$$

Here

$$c_x^e = \sqrt{\frac{\gamma p + c_0^2\rho_0 - (\gamma - 1)s_{xx}}{\rho} + \frac{4\mu}{3\rho}},\ c^s = \sqrt{\frac{\mu}{\rho}},\ c_y^e = \sqrt{\frac{\gamma p + c_0^2\rho_0 - (\gamma - 1)s_{yy}}{\rho} + \frac{4\mu}{3\rho}}.$$

The plastic solid satisfies the perfect plasticity assumption:

$$s_{xx}^2 + s_{yy}^2 + 2s_{xy}^2 + (s_{xx} + s_{yy})^2 \equiv \frac{2}{3}(Y_0)^2. \tag{5.4}$$

In the plastic solid model, we add the following equations for the deviatoric stresses and shear stress based on Reference [37].

$$\begin{aligned}
&\frac{\partial(\rho s_{xx})}{\partial t} + \frac{\partial(\rho u s_{xx})}{\partial x} + \frac{\partial(\rho v s_{xx})}{\partial y} = 0,\\
&\frac{\partial(\rho s_{yy})}{\partial t} + \frac{\partial(\rho u s_{yy})}{\partial x} + \frac{\partial(\rho v s_{yy})}{\partial y} = 0,\\
&\frac{\partial(\rho s_{xy})}{\partial t} + \frac{\partial(\rho u s_{xy})}{\partial x} + \frac{\partial(\rho v s_{xy})}{\partial y} = 0.
\end{aligned}$$

The governing equations for the plastic solid are therefore

$$\frac{\partial \mathbf{W}}{\partial t} + \frac{\partial \mathbf{F}(\mathbf{W})}{\partial x} + \frac{\partial \mathbf{G}(\mathbf{W})}{\partial y} = 0.$$

5.2. Split two-dimensional equations

We employ the dimensional splitting method for the two-dimensional problem. Without loss of generality, consider the equations in the y-direction:

$$\frac{\partial \mathbf{W}}{\partial t} + \mathbf{B}(\mathbf{W})\frac{\partial \mathbf{W}}{\partial y} = 0.$$

5.2.1. Paths for discontinuities

We use a linear path for an elastic shock wave or contact discontinuity with the left-hand state W_L and right-hand state W_R

$$\begin{aligned}
&\rho(s) = \rho_L + (\rho_R - \rho_L)s,\\
&(\rho u)(s) = (\rho u)_L + ((\rho u)_R - (\rho u)_L)s,\\
&(\rho v)(s) = (\rho v)_L + ((\rho v)_R - (\rho v)_L)s,\ \ s \in [0, 1].
\end{aligned} \tag{5.5}$$

Again, we use the symbol

$$\widetilde{\rho}_{L,R} = \begin{cases} \rho_L\rho_R \frac{[\![\ln\rho]\!]}{[\![\rho]\!]}, & \rho_L \neq \rho_R \\ \rho_L, & \rho_L = \rho_R \end{cases}$$

Based on the aforementioned path, we can compute the integral of non-conservative product directly, as follows.

$$\begin{aligned}
\int_0^1 \mathbf{B}\big(\Phi\big(s; \mathbf{W}_L, \mathbf{W}_R\big)\big)\frac{\partial \Phi}{\partial s}\big(s; \mathbf{W}_L, \mathbf{W}_R\big)\mathrm{d}s &= \mathbf{G}(\mathbf{W}_R) - \mathbf{G}(\mathbf{W}_L) + \begin{pmatrix} 0_{4\times 1} \\ \frac{2\mu}{3}\left(-[\![\rho]\!]\int_0^1 v(s)\mathrm{d}s + [\![\rho v]\!]\right) \\ \frac{4\mu}{3}\left([\![\rho]\!]\int_0^1 v(s)\mathrm{d}s - [\![\rho v]\!]\right) \\ \mu\left([\![\rho]\!]\int_0^1 u(s)\mathrm{d}s - [\![\rho u]\!]\right) \end{pmatrix} \\
&= \mathbf{G}(\mathbf{W}_R) - \mathbf{G}(\mathbf{W}_L) + \widetilde{\rho}_{L,R}\begin{pmatrix} 0_{4\times 1} \\ \frac{2\mu}{3}[\![v]\!] \\ -\frac{4\mu}{3}[\![v]\!] \\ -\mu[\![u]\!] \end{pmatrix}.
\end{aligned}$$

Let us consider the left-hand state W_L and right-hand state W_R constituting an admissible shock wave with the speed ς. From the Lax's entropy condition [32], we have

$$\text{there exists } k \in \{1, 2, 6, 7\} \text{ s.t. } \lambda_k(\mathbf{B}(\mathbf{W}_L)) > S > \lambda_k(\mathbf{B}(\mathbf{W}_R)). \tag{5.6}$$

Write

$$\eta = s_{xx} - \frac{2}{3}\mu\ln\rho,\ \ \xi = s_{yy} + \frac{4}{3}\mu\ln\rho.$$

For the split 2-D equations, we can also show that an admissible shock wave satisfy the Hooke's law in [38] under the path (5.5), i.e. $\eta =$ constant and $\xi =$ constant.

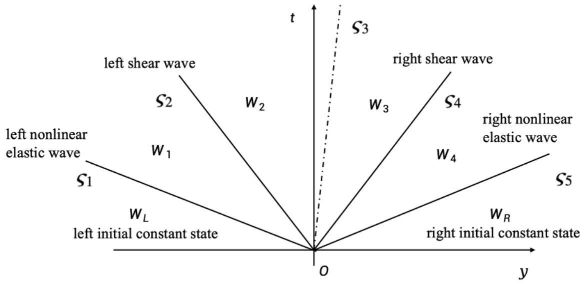

Fig. 3. Solution structure of Riemann problem for split two-dimensional equations for hypo-elastic solid in the y-axis.

Theorem 5.1. *Let the two states* $\mathbf{W}_L$ *and* $\mathbf{W}_R$ *satisfy the generalized Rankine-Hugoniot condition under the path* (5.5) *and the entropy condition* (5.6)*, then* $\eta_L = \eta_R$ *and* $\xi_L = \xi_R$.

Proof. The generalized Rankine-Hugoniot condition is

$$\mathbf{G}(\mathbf{W}_R) - \mathbf{G}(\mathbf{W}_L) + \widetilde{\rho}_{L,R}\Big(0_{4\times 1} \quad \tfrac{2\mu}{3}[\![v]\!] \quad -\tfrac{4\mu}{3}[\![v]\!] \quad -\mu[\![u]\!]\Big)^{\mathrm{T}} = \varsigma[\![\mathbf{W}]\!].$$

If $[\![\rho]\!] = 0$ and $\left[\!\left[s_{xx}\right]\!\right] = 0$, then it is obvious that $\eta_L = \eta_R$. If $[\![\rho]\!] = 0$ and $\left[\!\left[s_{xx}\right]\!\right] \neq 0$, then it follows from the R-H condition that

$$[\![v]\!] = \left[\!\left[s_{xy}\right]\!\right] = [\![u]\!] = \left[\!\left[s_{yy}\right]\!\right] = [\![p]\!] = 0, v_L = v_R = \varsigma.$$

Consequently, for any $k \in \{1, 2, 6, 7\}$, we have

$$\lambda_k(\mathbf{B}(\mathbf{W}_L)) = \lambda_k(\mathbf{B}(\mathbf{W}_R)),$$

which contracts the condition (5.6). We assume that $[\![\rho]\!] = 0$, then

$$\begin{aligned}
[\![\rho v \eta]\!] &= \left[\!\left[\rho v s_{xx}\right]\!\right] - \frac{2}{3}\mu[\![\rho v \ln \rho]\!] = \varsigma\left[\!\left[\rho s_{xx}\right]\!\right] - \frac{2}{3}\mu\widetilde{\rho}_{L,R}[\![v]\!] - \frac{2}{3}\mu[\![\rho v \ln \rho]\!] \\
&= \varsigma\left[\!\left[\rho s_{xx}\right]\!\right] - \frac{2}{3}\mu\big(\widetilde{\rho}_{L,R}[\![v]\!] + [\![\rho \ln \rho]\!]\{\{v\}\} + \{\{\rho \ln \rho\}\}[\![v]\!]\big) = \varsigma\left[\!\left[\rho s_{xx}\right]\!\right] - \frac{2}{3}\mu\left(\{\{\rho\}\}[\![v]\!]\frac{[\![\rho \ln \rho]\!]}{[\![\rho]\!]} + [\![\rho \ln \rho]\!]\{\{v\}\}\right) \\
&= \varsigma\left[\!\left[\rho s_{xx}\right]\!\right] - \frac{2}{3}\mu[\![\rho \ln \rho]\!]\left(\frac{\{\{\rho\}\}[\![v]\!] + \{\{v\}\}[\![\rho]\!]}{[\![\rho]\!]}\right) = \varsigma\left(\left[\!\left[\rho s_{xx}\right]\!\right] - \frac{2}{3}\mu[\![\rho \ln \rho]\!]\right) = \varsigma[\![\rho\eta]\!].
\end{aligned}$$

Substituting the first formula $[\![\rho v]\!] = \varsigma[\![\rho]\!]$ into the above equation, we have

$$[\![\eta]\!](\{\{\rho v\}\} - \varsigma\{\{\rho\}\}) = 0.$$

We asserts that $\{\{\rho v\}\} - \varsigma\{\{\rho\}\} \neq 0$. Otherwise, by the silmiliar method in the proof of Theorem 3.1, we can obtain that $[\![v]\!] = 0$ and $\varsigma = \{\{v\}\}$, which contracts the condition (5.6). The proof for ξ is similar. □

Finally, we consider the left-hand state W_L and the right-hand state W_R constituting an contact discontinuity with the speed ς. Based on the generalized R-H relation, we have the following conclusion.

Theorem 5.2. *Let the two states* $\mathbf{W}_L$ *and* $\mathbf{W}_R$ *satisfy the generalized Rankine-Hugoniot condition under the path* (5.5) *and* $v_L = v_R$*, then* $u_L = u_R$, $(s_{xy})_L = (s_{xy})_R$ *and* $(\sigma_{yy})_L = (\sigma_{yy})_R$.

As a result, the non-conservative product is zero, and

$$\int_0^1 \mathbf{B}\big(\Phi\big(s; \mathbf{W}_L, \mathbf{W}_R\big)\big)\frac{\partial \Phi}{\partial s}\big(s; \mathbf{W}_L, \mathbf{W}_R\big)\mathrm{d}s = \mathbf{G}(\mathbf{W}_R) - \mathbf{G}(\mathbf{W}_L).$$

5.2.2. Riemann solver

The path for arbitrary two states $\mathbf{W}_L$ and $\mathbf{W}_R$ is a piecewise mapping that is based on the solution of Riemann problem

$$\frac{\partial \mathbf{W}}{\partial t} + \mathbf{B}(\mathbf{W})\frac{\partial \mathbf{W}}{\partial y} = 0, \quad \mathbf{W}(x, y, t = 0) = \begin{cases} \mathbf{W}_L, & y < 0 \\ \mathbf{W}_R, & y \geq 0 \end{cases}$$

Fig. 3 illustrates the solution structure of this Riemann problem. The eigenvalues λ_1 and λ_7 correspond to the left and right nonlinear elastic waves, respectively, with the wave speeds represented by ς_1 and ς_5. The eigenvalues λ_3, λ_4 and λ_5 are linearly degenerate, and correspond to a contact discontinuity with its wave speed ς_3. The eigenvalues λ_2 and λ_6 correspond to the left and right shear waves with the wave speeds represented by ς_2 and ς_4, respectively. Furthermore, the variables $\mathbf{W}_K = [\mathbf{U}_K, s_{xx,K}, s_{yy,K}, s_{xy,K}]^T, K = L/R$, constitute the vector of initial states. The constant intermediate states on the left and right sides of the contact discontinuity are denoted by $\mathbf{W}_{2/3} = \left(\mathbf{U}_{2/3}, s_{xx,2/3}, s_{yy,2/3}, s_{xy,2/3}\right)^T$. $\mathbf{W}_{1/4} = \left(\mathbf{U}_{1/4}, s_{xx,1/4}, s_{yy,1/4}, s_{xy,1/4}\right)^T$ represents the shear wave front state. According to [38], u and s_{xy} are constant through the nonlinear elastic waves. In addition, ρ, s_{xx}, s_{yy} and v are all constant passing through the shear waves. In the vicinity of the contact discontinuity, u, v, s_{xy}, and σ_{yy} also remain unchanged.

To avoid the complexity of solving the exact Riemann solution, we consider an approximate Riemann solver again, which is characterized by Definition 3.1. Various existing elastic-plastic solid approximate solvers [38,39,46] are logically interpreted within this framework. When the generalized Rankine-Hugoniot condition of stress are not considered, ignoring shear waves results in the approximate solver proposed by Cheng et al. [38], whereas considering shear waves yields the solver proposed by Li et al. [39]. When the generalized Rankine-Hugoniot condition of stress are accounted for, ignoring both shear waves and contact discontinuities leads to a three-wave HLLEPJ Riemann solver. Ignoring only shear waves results in a three-wave HLLCEPJ Riemann solver, while considering both factors gives a five-wave HLLCEPJ Riemann solver. Numerical results in [46] show that, without accounting for strong shear, both the three-wave HLLCEPJ and five-wave HLLCEPJ solvers effectively capture elastic-plastic waves, with the three-wave HLLCEPJ solver offering a significantly simpler expression than the five-wave variant. The three-wave HLLCEPJ Riemann solver proposed in [46] is used in this paper:

$$\varsigma_1 = \min\left(v_L - c^e_{y,L}, v_R - c^e_{y,R}\right), \varsigma_2 = \min\left(v_L - c^s_L, v_R - c^s_R\right),$$

$$\varsigma_4 = \max\left(v_L + c^s_L, v_R + c^s_R\right), \varsigma_5 = \max\left(v_L + c^e_{y,L}, v_R + c^e_{y,R}\right).$$

$$\mathbf{W}_1: \quad \rho_1 = \rho_2, s_{xx,1} = s_{xx,2}, s_{yy,1} = s_{yy,2}, s_{xy,1} = s_{xy,L}, u_1 = u_L, v_1 = v_2, \sigma_2 = \sigma_1, E_1 = E_2.$$

$$\mathbf{W}_2: \quad \begin{aligned} \rho_2 &= \rho_L \frac{\varsigma_1 - v_L}{\varsigma_1 - v_2},\\ s_{xx,2} &= \frac{2\mu}{3}\ln\frac{\rho_1}{\rho_L} + s_{xx,L},\\ s_{yy,2} &= -\frac{4\mu}{3}\ln\frac{\rho_1}{\rho_L} + s_{yy,L},\\ s_{xy,2} &= \frac{(\varsigma_5 - v_2)s_{xy,R} - (\varsigma_1 - v_2)s_{xy,L} + \mu(u_R - u_L)}{\varsigma_5 - \varsigma_1},\\ u_2 &= \frac{s_{xy,R} - s_{xy,L} - \rho_1 u_L(\varsigma_2 - u_L) + \rho_4 u_R(\varsigma_4 - u_R)}{-\rho_0(\varsigma_2 - u_L) + \rho_4(\varsigma_4 - u_R)},\\ v_2 &= \frac{-\sigma_{yy,R} + \sigma_{yy,L} + \rho_L v_L(\varsigma_1 - v_L) + \rho_R v_R(\varsigma_5 - v_R)}{-\rho_L(\varsigma_1 - v_L) + \rho_R(\varsigma_5 - v_R)},\\ \sigma_2 &= \sigma_L - \rho_L(\varsigma_1 - v_L)(v_2 - v_L),\\ E_2 &= E_L + (v_2 - v_L)(v_2 - \sigma_{yy,L}/(\rho_L(\varsigma_1 - v_L))). \end{aligned}$$

$$\mathbf{W}_3: \quad \begin{aligned} \rho_3 &= \rho_R \frac{\varsigma_5 - v_R}{\varsigma_5 - v_3},\\ s_{xx,3} &= \frac{2\mu}{3}\ln\frac{\rho_3}{\rho_R} + s_{xx,R},\\ s_{yy,3} &= -\frac{4\mu}{3}\ln\frac{\rho_3}{\rho_R} + s_{yy,R},\\ s_{xy,3} &= s_{xy,2},\\ u_3 &= u_2,\\ v_3 &= v_2,\\ \sigma_3 &= \sigma_2,\\ E_3 &= E_R + (v_3 - v_R)(v_3 - \sigma_{yy,R}/(\rho_R(\varsigma_5 - v_R))). \end{aligned}$$

$$\mathbf{W}_4: \quad \rho_4 = \rho_3, s_{xx,4} = s_{xx,3}, s_{yy,4} = s_{yy,3}, s_{xy,4} = s_{xy,R} u_4 = u_R, v_4 = v_3, \sigma_4 = \sigma_3, E_4 = E_3.$$

5.3. Path-conservative finite volume method

We study the finite volume method for the two-dimensional hypo-elastic plastic problem on a bounded domain:

$$\begin{cases} \frac{\partial \mathbf{W}}{\partial t} + \mathbf{A}(\mathbf{W})\frac{\partial \mathbf{W}}{\partial x} + \mathbf{B}(\mathbf{W})\frac{\partial \mathbf{W}}{\partial y} = 0, & \text{if } s_{xx}^2 + s_{yy}^2 + 2s_{xy}^2 + (s_{xx} + s_{yy})^2 < \frac{2}{3}(Y_0)^2\\ \frac{\partial \mathbf{W}}{\partial t} + \frac{\partial \mathbf{F}(\mathbf{W})}{\partial x} + \frac{\partial \mathbf{G}(\mathbf{W})}{\partial y} = 0, & \text{otherwise} \end{cases}$$

$$\mathbf{W}(x,y,0) = \mathbf{W}_0(x,y), \quad (x,y) \in [a,b]\times[c,d],\ t \geq 0.$$

For simplicity, we restrict our consideration to a structured grid

$$a = x_{1/2} < \ldots < x_{i-1/2} < x_{i+1/2} < \ldots < x_{M+1/2} = b,$$

$$c = y_{1/2} < \ldots < y_{j-1/2} < y_{j+1/2} < \ldots < y_{N+1/2} = d,$$

$$x_{i+1/2} - x_{i-1/2} \equiv h_x,\ y_{j+1/2} - y_{j-1/2} \equiv h_y,\ h = \max(h_x, h_y).$$

In the time direction, we use a uniform discretization:

$$t^n = n\Delta t, \quad \Delta t \text{ is a constant.}$$

The time step size satisfies

$$\Delta t = \frac{CFL \cdot \Delta x}{\max_{1\leq k\leq 7}\lambda_k(\mathbf{W}_h)},\ CFL \leq \frac{1}{2}.$$

In the finite volume framework, we approximate the cell average of variables

$$\mathbf{W}^n_{i,j} \approx \int_{y_{j-1/2}}^{y_{j+1/2}}\int_{x_{i-1/2}}^{x_{i+1/2}} \mathbf{W}(x,y,t^n)\mathrm{d}x\mathrm{d}y,\ \mathbf{W}^0_{i,j} = \int_{y_{j-1/2}}^{y_{j+1/2}}\int_{x_{i-1/2}}^{x_{i+1/2}} \mathbf{W}_0(x,y)\mathrm{d}x\mathrm{d}y,$$

and the numerical solution is

$$\mathbf{W}_h(x,y,t) = 1_{[x_{i-1/2},x_{i+1/2})\times[y_{j-1/2},y_{j+1/2})\times[t^n,t^{n+1})}\mathbf{W}^n_{i,j}.$$

For any cell, if

$$s_{xx,h}^2 + s_{yy,h}^2 + 2s_{xy,h}^2 + (s_{xx,h} + s_{yy,h})^2 < \frac{2}{3}(Y_0)^2,$$

then we use the finite volume scheme for hypo-elastic solid, otherwise we use the scheme for plastic solid. The details are given as follows.

5.3.1. *Scheme for hypo-elastic solid model*

The path-conservative finite volume scheme for 2-D hypo-elastic solid model is

$$\mathbf{W}_{i,j}^{n+1} = \mathbf{W}_{i,j}^{n} - \frac{\Delta t}{h_x}\left(\mathbf{D}_{i-1/2,j}^{+} + \mathbf{D}_{i+1/2,j}^{-}\right) - \frac{\Delta t}{h_y}\left(\mathbf{D}_{i,j-1/2}^{+} + \mathbf{D}_{i,j+1/2}^{-}\right).$$

The numerical fluxes in the x-direction are

$$\mathbf{D}_{i+1/2,j}^{-} = \sum_{k=1}^{K} \min(\varsigma_k, 0)\left(\mathbf{F}(\mathbf{W}_{k+1}) - \mathbf{F}(\mathbf{W}_k) + \widetilde{\rho}_k \begin{pmatrix} 0_{4\times1} \\ -\frac{4\mu}{3}(u_{k+1} - u_k) \\ \frac{2\mu}{3}(u_{k+1} - u_k) \\ -\mu(v_{k+1} - v_k) \end{pmatrix}\right),$$

$$\mathbf{D}_{i+1/2,j}^{+} = \sum_{k=1}^{K} \max(\varsigma_k, 0)\left(\mathbf{F}(\mathbf{W}_{k+1}) - \mathbf{F}(\mathbf{W}_k) + \widetilde{\rho}_k \begin{pmatrix} 0_{4\times1} \\ -\frac{4\mu}{3}(u_{k+1} - u_k) \\ \frac{2\mu}{3}(u_{k+1} - u_k) \\ -\mu(v_{k+1} - v_k) \end{pmatrix}\right),$$

where the intermediate states $W_k (0 \le k \le K)$ and wave speeds $\varsigma_k (1 \le k \le K)$ are given by an Riemann solver of the Riemann problem

$$\frac{\partial \mathbf{W}}{\partial t} + \mathbf{A}(\mathbf{W})\frac{\partial \mathbf{W}}{\partial x} = 0, \quad \mathbf{W}(x, y, t = 0) = \begin{cases} \mathbf{W}_{i,j}^n, & x < 0 \\ \mathbf{W}_{i+1,j}^n, & x \ge 0 \end{cases}$$

and

$$\widetilde{\rho}_k = \begin{cases} \rho_k \rho_{k+1} \frac{\ln \rho_{k+1} - \ln \rho_k}{\rho_{k+1} - \rho_k}, & \rho_k \neq \rho_{k+1} \\ \rho_k, & \rho_k = \rho_{k+1} \end{cases} \tag{5.7}$$

The numerical fluxes in the y-direction, where we use the same notation for simplicity, are

$$\mathbf{D}_{i,j+1/2}^{-} = \sum_{k=1}^{K} \min(\varsigma_k, 0)\left(\mathbf{G}(\mathbf{W}_{k+1}) - \mathbf{G}(\mathbf{W}_k) + \widetilde{\rho}_k \begin{pmatrix} 0_{4\times1} \\ \frac{2\mu}{3}(v_{k+1} - v_k) \\ -\frac{4\mu}{3}(v_{k+1} - v_k) \\ -\mu(u_{k+1} - u_k) \end{pmatrix}\right),$$

$$\mathbf{D}_{i,j+1/2}^{+} = \sum_{k=1}^{K} \max(\varsigma_k, 0)\left(\mathbf{G}(\mathbf{W}_{k+1}) - \mathbf{G}(\mathbf{W}_k) + \widetilde{\rho}_k \begin{pmatrix} 0_{4\times1} \\ \frac{2\mu}{3}(v_{k+1} - v_k) \\ -\frac{4\mu}{3}(v_{k+1} - v_k) \\ -\mu(u_{k+1} - u_k) \end{pmatrix}\right),$$

where the intermediate states $W_k (0 \le k \le K)$ and wave speeds $\varsigma_k (1 \le k \le K)$ are given by an Riemann solver of the Riemann problem

$$\frac{\partial \mathbf{W}}{\partial t} + \mathbf{B}(\mathbf{W})\frac{\partial \mathbf{W}}{\partial y} = 0, \quad \mathbf{W}(x, y, t = 0) = \begin{cases} \mathbf{W}_{i,j}^n, & y < 0 \\ \mathbf{W}_{i,j+1}^n, & y \ge 0 \end{cases}$$

and $\widetilde{\rho}_k$ follows the formula (5.7).

5.3.2. *Scheme for plastic solid model*

We use a standard conservative finite volume scheme for the plastic solid model:

$$\mathbf{W}_i^{n+1} = \mathbf{W}_i^n - \frac{\Delta t}{h_x}\left(\mathbf{F}\left(\mathbf{W}_{i+1/2,j}^{n+1/2}\right) - \mathbf{F}\left(\mathbf{W}_{i-1/2,j}^{n+1/2}\right)\right) - \frac{\Delta t}{h_y}\left(\mathbf{G}\left(\mathbf{W}_{i,j+1/2}^{n+1/2}\right) - \mathbf{G}\left(\mathbf{W}_{i,j-1/2}^{n+1/2}\right)\right).$$

The construction formula for the plastic numerical flux is identical to that of the elastic case and is therefore omitted [38]. To preserve the perfectly plasticity assumption (5.4), we modify the deviator stress and shear stress at each time step. If

$$(s_{xx,i,j}^n)^2 + (s_{yy,i,j}^n)^2 + 2(s_{xy,i,j}^n)^2 + (s_{xx,i,j}^n + s_{yy,i,j}^n)^2 > \frac{2}{3}(Y_0)^2,$$

then we reassign the values of $\begin{pmatrix} s_{xx,i,j}^n & s_{yy,i,j}^n & s_{xy,i,j}^n \end{pmatrix}^{\mathrm{T}}$ using

$$\frac{\sqrt{\frac{2}{3}}Y_0}{\sqrt{(s_{xx,i,j}^n)^2 + (s_{yy,i,j}^n)^2 + 2(s_{xy,i,j}^n)^2 + (s_{xx,i,j}^n + s_{yy,i,j}^n)^2}} \begin{pmatrix} s_{xx,i,j}^n \\ s_{yy,i,j}^n \\ s_{xy,i,j}^n \end{pmatrix}.$$

Due to the unified nature of the adopted two-dimensional elastic-plastic model, we do not need to account for the transition between elastic and plastic states in the numerical solution, nor do we require special treatment for the numerical flux at the elastic-plastic interface.

6. Two-dimensional extension of the Jaumann correction

In this section, we consider a more refined two-dimensional elastic-plastic model as presented in [38,39,46,47]. This new model includes a Jaumann correction term in the deviatoric stress equation. Our method from the previous section can be extended directly to this model. The system, which maintains identical mass, momentum, and energy equations, is coupled with the deviatoric stress equation

$$
\begin{aligned}
&\frac{\partial(\rho s_{xx})}{\partial t}+\frac{\partial(\rho u s_{xx})}{\partial x}+\frac{\partial(\rho v s_{xx})}{\partial y}-\frac{2}{3}\mu\rho\left(2\frac{\partial u}{\partial x}-\frac{\partial v}{\partial y}\right)-\rho s_{xy}\left(\frac{\partial u}{\partial y}-\frac{\partial v}{\partial x}\right)=0,\\
&\frac{\partial(\rho s_{yy})}{\partial t}+\frac{\partial(\rho u s_{yy})}{\partial x}+\frac{\partial(\rho v s_{yy})}{\partial y}-\frac{2}{3}\mu\rho\left(2\frac{\partial v}{\partial y}-\frac{\partial u}{\partial x}\right)+\rho s_{xy}\left(\frac{\partial u}{\partial y}-\frac{\partial v}{\partial x}\right)=0,\\
&\frac{\partial(\rho s_{xy})}{\partial t}+\frac{\partial(\rho u s_{xy})}{\partial x}+\frac{\partial(\rho v s_{xy})}{\partial y}-\mu\rho\left(\frac{\partial v}{\partial x}+\frac{\partial u}{\partial y}\right)+\frac{1}{2}\rho\left(s_{xx}-s_{yy}\right)\left(\frac{\partial u}{\partial y}-\frac{\partial v}{\partial x}\right)=0.
\end{aligned}
\tag{6.1}
$$

We also utilize the dimensional splitting method for the two-dimensional problem. For simplicity, we employ the same symbols, and the governing equations for the elastic-plastic solid in the y-direction are stated as follows:

$$
\begin{aligned}
&\frac{\partial \mathbf{W}}{\partial t}+\mathbf{B}(\mathbf{W})\frac{\partial \mathbf{W}}{\partial y}=0,\\
&\mathbf{W}=\begin{pmatrix}\rho & \rho u & \rho v & E & \rho s_{xx} & \rho s_{yy} & \rho s_{xy}\end{pmatrix}^{\mathrm{T}},\\
&\mathbf{B}(\mathbf{W})=\frac{\partial \mathbf{G}(\mathbf{W})}{\partial \mathbf{W}}+\begin{pmatrix} & & & 0_{4\times 7} & & & \\ -\frac{2\mu v}{3} & 0 & \frac{2\mu}{3} & 0 & 0 & 0 & 0\\ \frac{4\mu v}{3} & 0 & -\frac{4\mu}{3} & 0 & 0 & 0 & 0\\ \mu u & -\mu & 0 & 0 & 0 & 0 & 0\end{pmatrix}+\underbrace{\begin{pmatrix} & & & 0_{4\times 7} & & & \\ s_{xy}u & -s_{xy} & 0 & 0 & 0 & 0 & 0\\ -s_{xy}u & s_{xy} & 0 & 0 & 0 & 0 & 0\\ -\frac{1}{2}\left(s_{xx}-s_{yy}\right)u & \frac{1}{2}\left(s_{xx}-s_{yy}\right) & 0 & 0 & 0 & 0 & 0\end{pmatrix}}_{\text{Jaumann correction}}.
\end{aligned}
$$

6.1. Paths for discontinuity

We continue to use the straight-line path for both density and momentum

$$
\begin{aligned}
\rho(s;\mathbf{W}_L,\mathbf{W}_R)&=\rho_L+(\rho_R-\rho_L)s,\\
(\rho u)(s;\mathbf{W}_L,\mathbf{W}_R)&=(\rho u)_L+((\rho u)_R-(\rho u)_L)s,\\
(\rho v)(s;\mathbf{W}_L,\mathbf{W}_R)&=(\rho v)_L+((\rho v)_R-(\rho v)_L)s,\ \ s\in[0,1],
\end{aligned}
\tag{6.2}
$$

As a result, the integral of the Jaumann correction part is

$$
\begin{aligned}
&\int_0^1\begin{pmatrix} & & & 0_{4\times 7} & & & \\ s_{xy}u & -s_{xy} & 0 & 0 & 0 & 0 & 0\\ -s_{xy}u & s_{xy} & 0 & 0 & 0 & 0 & 0\\ -\frac{1}{2}\left(s_{xx}-s_{yy}\right)u & \frac{1}{2}\left(s_{xx}-s_{yy}\right) & 0 & 0 & 0 & 0 & 0\end{pmatrix}\frac{\partial \Phi}{\partial s}\left(s;\mathbf{W}_L,\mathbf{W}_R\right)\mathrm{d}s\\
&=\begin{pmatrix} 0_{4\times 1}\\ [\![\rho]\!]\int_0^1 s_{xy}(s)u(s)\mathrm{d}s-[\![\rho u]\!]\int_0^1 s_{xy}(s)\mathrm{d}s\\ -[\![\rho]\!]\int_0^1 s_{xy}(s)u(s)\mathrm{d}s+[\![\rho u]\!]\int_0^1 s_{xy}(s)\mathrm{d}s\\ -\frac{1}{2}[\![\rho]\!]\int_0^1\left(s_{xx}(s)-s_{yy}(s)\right)u(s)\mathrm{d}s+\frac{1}{2}[\![\rho u]\!]\int_0^1\left(s_{xx}(s)-s_{yy}(s)\right)\mathrm{d}s\end{pmatrix}.
\end{aligned}
\tag{6.3}
$$

We observe that in the Riemann solution, the nonlinear elastic waves and contact discontinuities exhibit a continuous velocity u, i.e., $[\![u]\!]=0$. Consequently, that integral does not depend on the path for deviatoric stress and is equal to zero. The integral of the non-conservative part is therefore

$$
\int_0^1\mathbf{B}\left(\Phi\left(s;\mathbf{W}_L,\mathbf{W}_R\right)\right)\frac{\partial \Phi}{\partial s}\left(s;\mathbf{W}_L,\mathbf{W}_R\right)\mathrm{d}s=\mathbf{G}(\mathbf{W}_R)-\mathbf{G}(\mathbf{W}_L)+\widetilde{\rho}_{L,R}\begin{pmatrix}0_{4\times 1}\\ \frac{2\mu}{3}[\![v]\!]\\ -\frac{4\mu}{3}[\![v]\!]\\ -\mu[\![u]\!]\end{pmatrix},
\tag{6.4}
$$

and the Hooke's law presented in Theorem 5.1 will still be valid. For the discontinuity with $[\![u]\!]\neq 0$, the integral of the non-conservative product depends on the path for deviatoric stress. We use the straight-line path for s_{xx}, s_{yy}, and s_{xy} in [46]:

$$
\begin{aligned}
s_{xx}(s;\mathbf{W}_L,\mathbf{W}_R)&=s_{xx,L}+(s_{xx,R}-s_{xx,L})s,\\
s_{yy}(s;\mathbf{W}_L,\mathbf{W}_R)&=s_{yy,L}+(s_{yy,R}-s_{yy,L})s,\\
s_{xy}(s;\mathbf{W}_L,\mathbf{W}_R)&=s_{xy,L}+(s_{xy,R}-s_{xy,L})s,\ \ s\in[0,1].
\end{aligned}
\tag{6.5}
$$

Under this path, we have

$$\int_0^1 s_{xy}(s)\mathrm{d}s = \{\{s_{xy}\}\},\ \int_0^1 s_{xx}(s)\mathrm{d}s = \{\{s_{xx}\}\},\ \int_0^1 s_{yy}(s)\mathrm{d}s = \{\{s_{yy}\}\}.$$

It is commonly assumed that $[\![\rho]\!] = 0$ for shear waves in the Riemann solution. Therefore, we have

$$\int_0^1 \begin{pmatrix} & & & 0_{4\times7} & & & \\ s_{xy}u & -s_{xy} & 0 & 0 & 0 & 0 & 0 \\ -s_{xy}u & s_{xy} & 0 & 0 & 0 & 0 & 0 \\ -\frac{1}{2}(s_{xx}-s_{yy})u & \frac{1}{2}(s_{xx}-s_{yy}) & 0 & 0 & 0 & 0 & 0 \end{pmatrix} \frac{\partial\Phi}{\partial s}(s;\mathbf{W}_L,\mathbf{W}_R)\mathrm{d}s = [\![\rho u]\!]\begin{pmatrix} 0_{4\times1} \\ -\{\{s_{xy}\}\} \\ \{\{s_{xy}\}\} \\ \frac{1}{2}(\{\{s_{xx}\}\}-\{\{s_{yy}\}\}) \end{pmatrix}$$

and

$$\int_0^1 \mathbf{B}(\Phi(s;\mathbf{W}_L,\mathbf{W}_R))\frac{\partial\Phi}{\partial s}(s;\mathbf{W}_L,\mathbf{W}_R)\mathrm{d}s = \mathbf{G}(\mathbf{W}_R)-\mathbf{G}(\mathbf{W}_L)+\widetilde{\rho}_{L,R}\begin{pmatrix} 0_{4\times1} \\ \frac{2\mu}{3}[\![v]\!] \\ -\frac{4\mu}{3}[\![v]\!] \\ -\mu[\![u]\!] \end{pmatrix} + \underbrace{[\![\rho u]\!]\begin{pmatrix} 0_{4\times1} \\ -\{\{s_{xy}\}\} \\ \{\{s_{xy}\}\} \\ \frac{1}{2}(\{\{s_{xx}\}\}-\{\{s_{yy}\}\}) \end{pmatrix}}_{\text{Jaumann correction}}. \tag{6.6}$$

For more general discontinuities, the integral can become complicated. By substituting the following formula into the integral for the Jaumann correction part, we can complete the integral for the non-conservative part.

$$\begin{aligned}
&\int_0^1 s_{xx}(s)u(s)\mathrm{d}s \\
=&\frac{[\![\rho u]\!]}{2[\![\rho]\!]}+\frac{[\![\rho]\!]((\rho u)_L[\![s_{xx}]\!]+[\![\rho u]\!]s_{xx,L})-[\![\rho u]\!][\![s_{xx}]\!]\rho_L}{[\![\rho]\!]^2}+\frac{([\![\rho u]\!]\rho_L-(\rho u)_L[\![\rho]\!])([\![s_{xx}]\!]\rho_L-s_{xx,L}[\![\rho]\!])}{[\![\rho]\!]^3}\ln\left|1+\frac{[\![\rho]\!]}{\rho_L}\right|, \\
&\int_0^1 s_{yy}(s)u(s)\mathrm{d}s \\
=&\frac{[\![\rho u]\!]}{2[\![\rho]\!]}+\frac{[\![\rho]\!]((\rho u)_L[\![s_{yy}]\!]+[\![\rho u]\!]s_{yy,L})-[\![\rho u]\!][\![s_{yy}]\!]\rho_L}{[\![\rho]\!]^2}+\frac{([\![\rho u]\!]\rho_L-(\rho u)_L[\![\rho]\!])([\![s_{yy}]\!]\rho_L-s_{yy,L}[\![\rho]\!])}{[\![\rho]\!]^3}\ln\left|1+\frac{[\![\rho]\!]}{\rho_L}\right|, \\
&\int_0^1 s_{xy}(s)u(s)\mathrm{d}s \\
=&\frac{[\![\rho u]\!]}{2[\![\rho]\!]}+\frac{[\![\rho]\!]((\rho u)_L[\![s_{xy}]\!]+[\![\rho u]\!]s_{xy,L})-[\![\rho u]\!][\![s_{xy}]\!]\rho_L}{[\![\rho]\!]^2}+\frac{([\![\rho u]\!]\rho_L-(\rho u)_L[\![\rho]\!])([\![s_{xy}]\!]\rho_L-s_{xy,L}[\![\rho]\!])}{[\![\rho]\!]^3}\ln\left|1+\frac{[\![\rho]\!]}{\rho_L}\right|.
\end{aligned}$$

6.2. Riemann solver

The numerical flux is based on an approximate Riemann solver of the extended model (6.1). Compared to the previous model, the values of s_{xx}, s_{yy}, and s_{xy} are needed in the intermediate regions $\mathbf{W}_{2,3}$ for the new model. We utilize the HLLCEPJ Riemann solver introduced by Serezhkin [46]:

$$\begin{aligned}
&\varsigma_1 = \min\left(v_L - c^e_{y,L}, v_R - c^e_{y,R}\right),\ \varsigma_2 = \min\left(v_L - c^s_L, v_R - c^s_R\right), \\
&\varsigma_4 = \max\left(v_L + c^s_L, v_R + c^s_R\right),\ \varsigma_5 = \max\left(v_L + c^e_{y,L}, v_R + c^e_{y,R}\right).
\end{aligned}$$

$$\mathbf{W}_1: \quad \rho_1=\rho_2,\ s_{xx,1}=\frac{2\mu}{3}\ln\frac{\rho_1}{\rho_L}+s_{xx,L},\ s_{yy,1}=-\frac{4\mu}{3}\ln\frac{\rho_1}{\rho_L}+s_{yy,L},\ s_{xy,1}=s_{xy,L},\ u_1=u_L,\ v_1=v_2,\ \sigma_2=\sigma_1,\ E_1=E_2.$$

$$\begin{aligned}
\mathbf{W}_2: \quad &\rho_2=\rho_L\frac{\varsigma_1-v_L}{\varsigma_1-v_2}, \\
&u_2=\frac{s_{xy,R}-s_{xy,L}-\rho_1 u_L(\varsigma_2-u_L)+\rho_4 u_R(\varsigma_4-u_R)}{-\rho_0(\varsigma_2-u_L)+\rho_4(\varsigma_4-u_R)}, \\
&v_2=\frac{-\sigma_{yy,R}+\sigma_{yy,L}+\rho_L v_L(\varsigma_1-v_L)+\rho_R v_R(\varsigma_5-v_R)}{-\rho_L(\varsigma_1-v_L)+\rho_R(\varsigma_5-v_R)}, \\
&\sigma_2=\sigma_L-\rho_L(\varsigma_1-v_L)(v_2-v_L), \\
&E_2=E_L+(v_2-v_L)(v_2-\sigma_{yy,L}/(\rho_L(\varsigma_1-v_L))).
\end{aligned}$$

$$\begin{aligned}
\mathbf{W}_3: \quad &\rho_3=\rho_R\frac{\varsigma_5-v_R}{\varsigma_5-v_3}, \\
&u_3=u_2, \\
&v_3=v_2, \\
&\sigma_3=\sigma_2, \\
&E_3=E_R+(v_3-v_R)(v_3-\sigma_{yy,R}/(\rho_R(\varsigma_5-v_R))).
\end{aligned}$$

$$\mathbf{W}_4: \quad \rho_4=\rho_3,\ s_{xx,4}=\frac{2\mu}{3}\ln\frac{\rho_3}{\rho_R}+s_{xx,R},\ s_{yy,4}=-\frac{4\mu}{3}\ln\frac{\rho_3}{\rho_R}+s_{yy,R},\ s_{xy,4}=s_{xy,R},\ u_4=u_R,\ v_4=v_3,\ \sigma_4=\sigma_3,\ E_4=E_3.$$

with

$$
\begin{aligned}
s_{xx,2} &= \frac{1}{(u_2-u_L)^2+4(-\varsigma_1+v_2)^2}\left(-2\mu(u_2-u_L)^2+4(-\varsigma_1+v_2)^2 s_{xx,1}+(u_2-u_L)^2 s_{yy,1}-4s_{xy,L}(-\varsigma_1+v_2)(u_2-u_L)\right),\\
s_{yy,2} &= \frac{1}{(u_2-u_L)^2+4(-\varsigma_1+v_2)^2}\left(2\mu(u_2-u_L)^2+4(-\varsigma_1+v_2)^2 s_{yy,1}+(u_2-u_L)^2 s_{xx,1}+4s_{xy,L}(-\varsigma_1+v_2)(u_2-u_L)\right),\\
s_{xy,2} &= \frac{1}{(u_2-u_L)^2+4(-\varsigma_1+v_2)^2}\left((4\mu+2s_{xx,1}-2s_{yy,1})(-\varsigma_1+v_2)(u_2-u_L)+s_{xy,L}(2v_2+u_2-2\varsigma_1-u_L)(2v_2-u_2-2\varsigma_1+u_L)\right),
\end{aligned}
$$

$$
\begin{aligned}
s_{xx,3} &= \frac{1}{(u_3-u_R)^2+4(-\varsigma_5+v_3)^2}\left(-2\mu(u_3-u_R)^2+4(-\varsigma_5+v_3)^2 s_{xx,4}+(u_3-u_R)^2 s_{yy,4}-4s_{xy,R}(-\varsigma_5+v_3)(u_3-u_R)\right),\\
s_{yy,3} &= \frac{1}{(u_3-u_R)^2+4(-\varsigma_5+v_3)^2}\left(2\mu(u_3-u_R)^2+4(-\varsigma_5+v_3)^2 s_{yy,4}+(u_3-u_R)^2 s_{xx,4}+4s_{xy,R}(-\varsigma_5+v_3)(u_3-u_R)\right),\\
s_{xy,3} &= \frac{1}{(u_3-u_R)^2+4(-\varsigma_5+v_3)^2}\left((4\mu+2s_{xx,4}-2s_{yy,4})(-\varsigma_5+v_3)(u_3-u_R)+s_{xy,R}(2v_3+u_3-2\varsigma_5-u_R)(2v_3-u_3-2\varsigma_5+u_R)\right).
\end{aligned}
$$

In this Riemann solver, it holds that $[\![u]\!]=0$ for the two nonlinear elastic waves, and $[\![\rho]\!]=0$ for the two shear waves. Consequently, we can use the simple formulas (6.4) and (6.6) to compute the non-conservative part.

6.3. Path-conservative finite volume method

Taking into account the Jaumann correction, the appropriate path-conservative finite volume scheme is outlined as follows:

$$
\mathbf{W}_{i,j}^{n+1}=\mathbf{W}_{i,j}^{n}-\frac{\Delta t}{h_x}\left(\mathbf{D}^{+}_{i-1/2,j}+\mathbf{D}^{-}_{i+1/2,j}\right)-\frac{\Delta t}{h_y}\left(\mathbf{D}^{+}_{i,j-1/2}+\mathbf{D}^{-}_{i,j+1/2}\right).
$$

The numerical fluxes in the x-direction are

$$
\begin{aligned}
\mathbf{D}^{-}_{i+1/2,j} = &\sum_{k=1}^{K}\min(\varsigma_k,0)\left(\mathbf{F}(\mathbf{W}_{k+1})-\mathbf{F}(\mathbf{W}_k)+\widetilde{\rho}_k\begin{pmatrix}0_{4\times1}\\ -\frac{4\mu}{3}(u_{k+1}-u_k)\\ \frac{2\mu}{3}(u_{k+1}-u_k)\\ -\mu(v_{k+1}-v_k)\end{pmatrix}\right)\\
&+\sum_{k=2,4}\min(\varsigma_k,0)\left(\frac{\rho_{k+1}v_{k+1}-\rho_k v_k}{2}\begin{pmatrix}0_{4\times1}\\ s_{xy,k+1}+s_{xy,k}\\ -(s_{xy,k+1}+s_{xy,k})\\ -\frac{1}{2}\left(s_{xx,k+1}-s_{yy,k+1}+s_{xx,k}-s_{yy,k}\right)\end{pmatrix}\right),
\end{aligned}
$$

$$
\begin{aligned}
\mathbf{D}^{+}_{i+1/2,j} = &\sum_{k=1}^{K}\max(\varsigma_k,0)\left(\mathbf{F}(\mathbf{W}_{k+1})-\mathbf{F}(\mathbf{W}_k)+\widetilde{\rho}_k\begin{pmatrix}0_{4\times1}\\ -\frac{4\mu}{3}(u_{k+1}-u_k)\\ \frac{2\mu}{3}(u_{k+1}-u_k)\\ -\mu(v_{k+1}-v_k)\end{pmatrix}\right)\\
&+\sum_{k=2,4}\max(\varsigma_k,0)\left(\frac{\rho_{k+1}v_{k+1}-\rho_k v_k}{2}\begin{pmatrix}0_{4\times1}\\ s_{xy,k+1}+s_{xy,k}\\ -(s_{xy,k+1}+s_{xy,k})\\ -\frac{1}{2}\left(s_{xx,k+1}-s_{yy,k+1}+s_{xx,k}-s_{yy,k}\right)\end{pmatrix}\right),
\end{aligned}
$$

where the intermediate states $W_k(0\le k\le K)$ and wave speeds $\varsigma_k(1\le k\le K)$ are given by a Riemann solver of the Riemann problem

$$
\frac{\partial\mathbf{W}}{\partial t}+\mathbf{A}(\mathbf{W})\frac{\partial\mathbf{W}}{\partial x}=0,\quad \mathbf{W}(x,y,t=0)=\begin{cases}\mathbf{W}^n_{i,j}, & x<0\\ \mathbf{W}^n_{i+1,j}, & x\ge 0\end{cases}
$$

and $\widetilde{\rho}_k$ are given by (5.7).

The numerical fluxes in the y-direction are

$$\mathbf{D}^{-}_{i,j+1/2} = \sum_{k=1}^{K} \min(\varsigma_k, 0)\left(\mathbf{G}(\mathbf{W}_{k+1}) - \mathbf{G}(\mathbf{W}_k) + \widetilde{\rho}_k \begin{pmatrix} 0_{4\times1} \\ \frac{2\mu}{3}(v_{k+1} - v_k) \\ -\frac{4\mu}{3}(v_{k+1} - v_k) \\ -\mu(u_{k+1} - u_k) \end{pmatrix}\right)$$

$$+ \sum_{k=2,4} \min(\varsigma_k, 0)\left(\frac{\rho_{k+1}u_{k+1} - \rho_k u_k}{2}\begin{pmatrix} 0_{4\times1} \\ -(s_{xy,k+1} + s_{xy,k}) \\ s_{xy,k+1} + s_{xy,k} \\ \frac{1}{2}\left(s_{xx,k+1} - s_{yy,k+1} + s_{xx,k} - s_{yy,k}\right) \end{pmatrix}\right),$$

$$\mathbf{D}^{+}_{i,j+1/2} = \sum_{k=1}^{K} \max(\varsigma_k, 0)\left(\mathbf{G}(\mathbf{W}_{k+1}) - \mathbf{G}(\mathbf{W}_k) + \widetilde{\rho}_k \begin{pmatrix} 0_{4\times1} \\ \frac{2\mu}{3}(v_{k+1} - v_k) \\ -\frac{4\mu}{3}(v_{k+1} - v_k) \\ -\mu(u_{k+1} - u_k) \end{pmatrix}\right)$$

$$+ \sum_{k=2,4} \max(\varsigma_k, 0)\left(\frac{\rho_{k+1}u_{k+1} - \rho_k u_k}{2}\begin{pmatrix} 0_{4\times1} \\ -(s_{xy,k+1} + s_{xy,k}) \\ s_{xy,k+1} + s_{xy,k} \\ \frac{1}{2}\left(s_{xx,k+1} - s_{yy,k+1} + s_{xx,k} - s_{yy,k}\right) \end{pmatrix}\right),$$

where the intermediate states $W_k (0 \le k \le K)$ and wave speeds $\varsigma_k (1 \le k \le K)$ are given by a Riemann solver of the Riemann problem

$$\frac{\partial \mathbf{W}}{\partial t} + \mathbf{B}(\mathbf{W})\frac{\partial \mathbf{W}}{\partial y} = 0, \quad \mathbf{W}(x, y, t = 0) = \begin{cases} \mathbf{W}^n_{i,j}, & y < 0 \\ \mathbf{W}^n_{i,j+1}, & y \ge 0 \end{cases}$$

and $\widetilde{\rho}_k$ follows the formula (5.7).

We employ the methods detailed in [38,39,46] to address the elastic-plastic transition. Since both the elastic and plastic media are governed by equations of the same form, we do not need to modify the governing equations for this two-dimensional model. When the medium transitions from an elastic state to a plastic state, we will apply a radial return method for the stress tensor to ensure that the stress remains on the yield surface. More precisely, if

$$(s^{n+1}_{xx,i,j})^2 + (s^{n+1}_{yy,i,j})^2 + 2(s^{n+1}_{xy,i,j})^2 + (s^{n+1}_{xx,i,j} + s^{n+1}_{yy,i,j})^2 > \frac{2}{3}(Y_0)^2,$$

then we reassign the values of $\left(s^{n+1}_{xx,i,j} \quad s^{n+1}_{yy,i,j} \quad s^{n+1}_{xy,i,j}\right)^{\mathrm{T}}$ using

$$\frac{\sqrt{\frac{2}{3}}Y_0}{\sqrt{(s^{n+1}_{xx,i,j})^2 + (s^{n+1}_{yy,i,j})^2 + 2(s^{n+1}_{xy,i,j})^2 + (s^{n+1}_{xx,i,j} + s^{n+1}_{yy,i,j})}}\begin{pmatrix} s^{n+1}_{xx,i,j} \\ s^{n+1}_{yy,i,j} \\ s^{n+1}_{xy,i,j} \end{pmatrix}.$$

7. Numerical tests

In the following numerical tests, the solid material is aluminum with physical constant parameters $\gamma = 2.67, c_0 = 5380.0m/s, \rho_0 = 2710.0kg/m^3$, $\mathrm{K}=7400.0\mathrm{MPa}$, $\mu = 2650.0MPa, \mathrm{Y}_0 = 300.0MPa$. After the nondimensionalization, these parameters are transformed into $\gamma = 2.67$, $c_0 = 538.0, \rho_0 = 2.71$, $\mathrm{K} = 740000.0$, $\mu = 265000, \mathrm{Y}_0 = 3000.0$. The computational domain is set to be $[0.0, 4.0]$ with 1000 uniform grid points. Besides, the CFL number is 0.3. Below, in the figures, the legends of **PC-HLLC**, **PC-LSRS**, and **Ref** represent the numerical results simulated with path-conservative scheme with HLLC solver, LSRS method, and reference solution (Lax-Friedrichs scheme with 50000 uniform grid points) respectively.

7.1. One dimensional elastic problem

In this subsection, we introduce numerical examples of complex stress interactions to verify whether the proposed method can effectively capture the corresponding shock waves. Similar examples are also computed in Reference [14].

Test 1. The first test is the interaction of shock waves and is shown in Fig. 4. The nondimensional terminal time is 0.002, and the nondimensional initial conditions are

$$\begin{cases} u_L = 1.0, \quad \mathrm{p}_L = 1.0, \quad \mathrm{s}_L = -200.0, \quad \rho_L = 2.7 \\ u_{mid} = 1.0, \quad \mathrm{p}_{mid} = 1.0, \quad \mathrm{s}_{mid} = 400.0, \quad \rho_{mid} = 2.7 \\ u_R = -1.0, \quad \mathrm{p}_R = 1.0, \quad \mathrm{s}_R = -800.0, \quad \rho_R = 2.7 \end{cases}$$

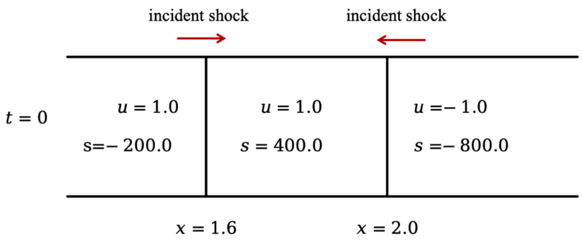

Fig. 4. The initial profile of Test 1.

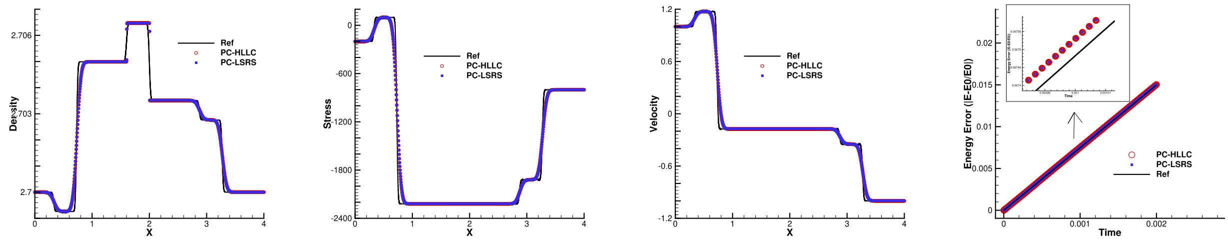

(a) Density (b) Stress (c) Velocity (d) Energy error(Test 1)

Fig. 5. The numerical solutions of path-conservative scheme for Test 1.

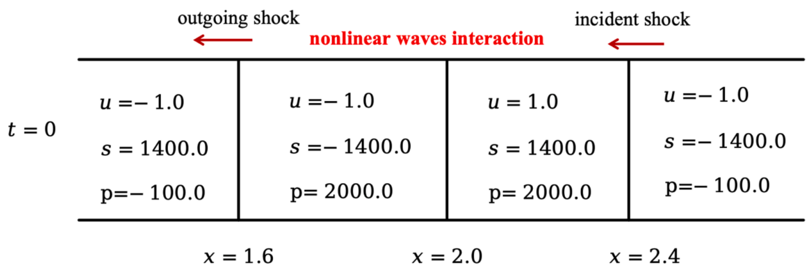

Fig. 6. The initial profile of Test 2.

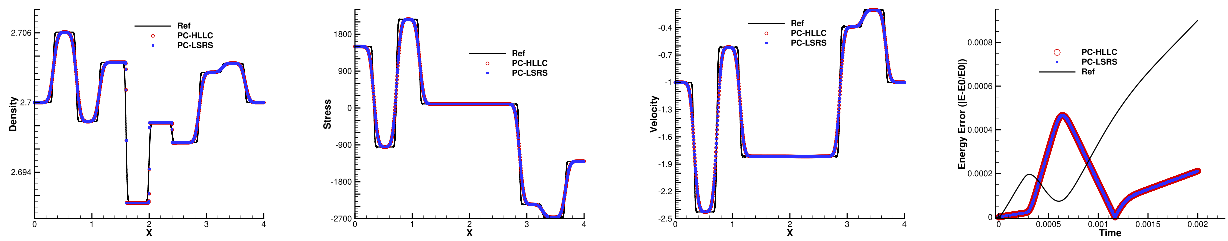

(a) Density (b) Stress (c) Velocity (d) Energy error(Test 2)

Fig. 7. The numerical solutions of path-conservative scheme for Test 2.

Test 2. In this example, more complex nonlinear elastic wave interactions are considered. The initial interfaces are located at $x_0 = 1.6$, $x_0 = 2.0$, and $x_0 = 2.4$, as illustrated in Fig. 6. The nondimensional terminal time is 0.0015, and the nondimensional initial conditions are

$$\begin{cases} u_L = -1.0, \quad p_L = -100.0, \quad s_L = 1400.0, \quad \rho_L = 2.7 \\ u_{midleft} = -1.0, \quad p_{midleft} = 2000.0, \quad s_{midleft} = -1400.0, \quad \rho_{midleft} = 2.7 \\ u_{midright} = 1.0, \quad p_{midright} = 2000.0, \quad s_{midright} = 1400.0, \quad \rho_{midright} = 2.7 \\ u_R = -1.0, \quad p_R = -100.0, \quad s_R = -1400.0, \quad \rho_R = 2.7 \end{cases}$$

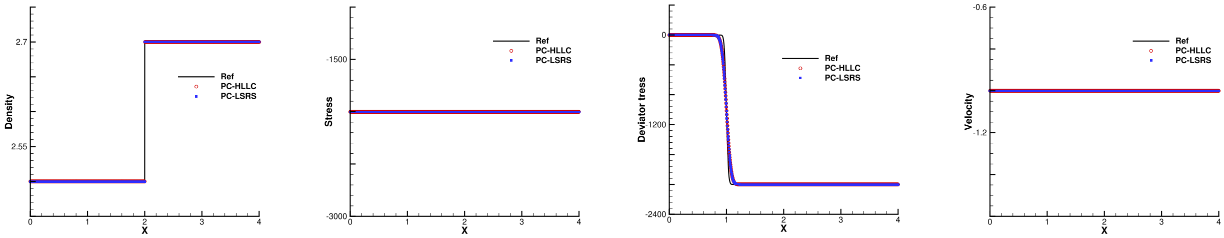

(a) Density (b) Stress (c) Deviatoric stress (d) Velocity

Fig. 8. The numerical solutions of path-conservative scheme for Test 3.

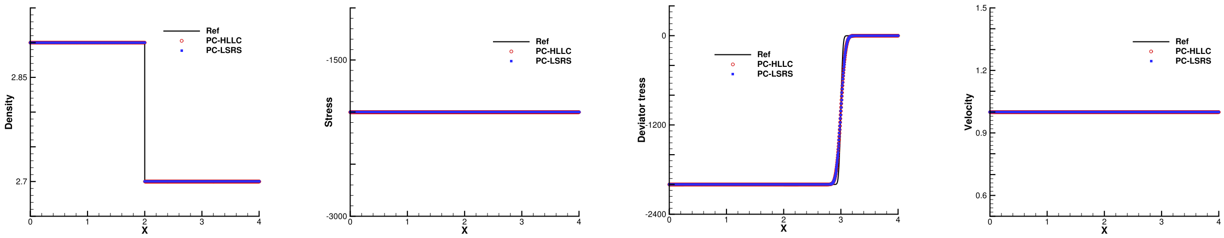

(a) Density (b) Stress (c) Deviatoric stress (d) Velocity

Fig. 9. The numerical solutions of path-conservative scheme for Test 4.

Table 1
The errors of numerical solutions in L_1 norm for Test 3 and Test 4.

Case	Method	Density	Velocity	Stress	Deviatoric Stress
Test 3	PC-HLLC				
	L_1 Norm	6.07921e-08	8.52078e-08	1.40949e-04	50.2307
	PC-LSRS				
	L_1 Norm	6.85471e-15	4.95881e-13	7.66968e-10	50.2307
Test 4	PC-HLLC				
	L_1 Norm	1.70914e-06	0.0004026	0.691791	50.2981
	PC-LSRS				
	L_1 Norm	5.88524e-13	4.53226e-12	6.37021e-09	50.1908

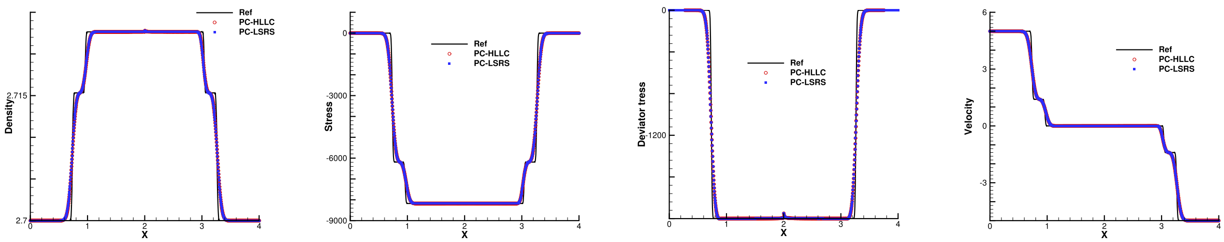

(a) Density (b) Stress (c) Deviatoric stress (d) Velocity

Fig. 10. The numerical solutions of path-conservative scheme for Test 5 with 1000 cells.

Figs. 5 and 7 show the density, stress, velocity, and temporal variation of the energy errors. With the numerical solutions of the elastic state $\overline{\mathbf{W}}_h$, the energy is computed as

$$E_h = \frac{s_h - \sigma_h - c_0^2(\rho_h - \rho_0)}{\gamma - 1} + \frac{1}{2}\rho_h u_h^2$$

which follows the equations of state for the plastic medium. The relative energy error is defined by

$$\left| \frac{\int_a^b E_h(x,t)\mathrm{d}x - \int_a^b E_h(x,0)\mathrm{d}x}{\int_a^b E_h(x,0)\mathrm{d}x} \right|.$$

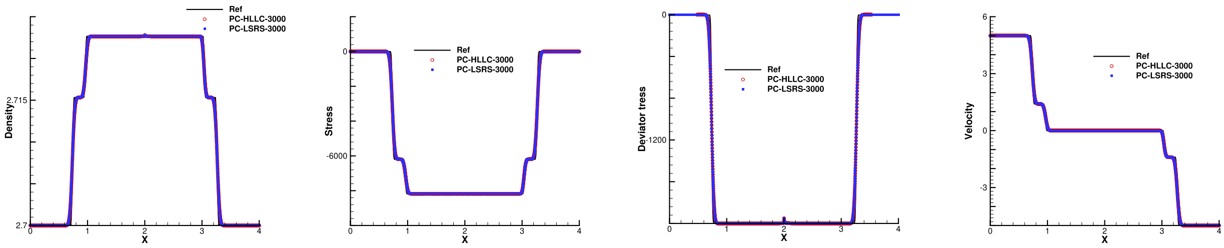

(a) Density (b) Stress (c) Deviatoric stress (d) Velocity

Fig. 11. The numerical solutions of path-conservative scheme for Test 5 with 3000 cells.

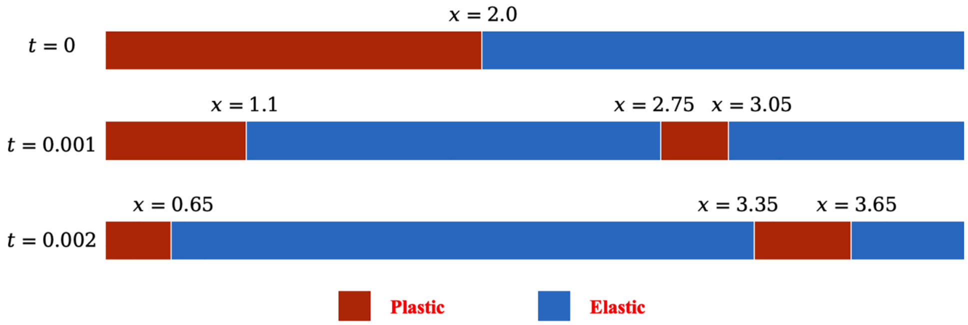

Fig. 12. The illustration of elastic-plastic region variations of Test 6.

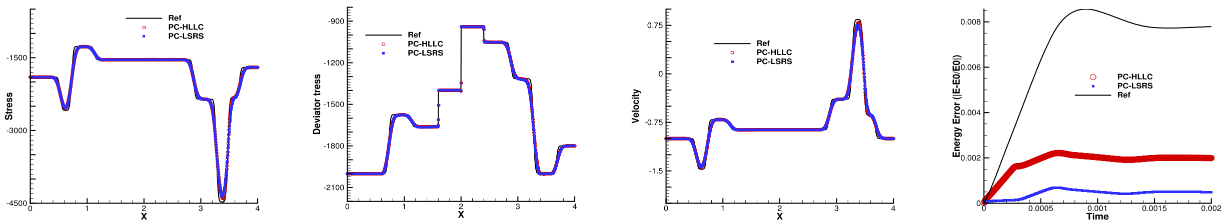

(a) Stress (b) Deviatoric stress (c) Velocity (d) Energy error

Fig. 13. The numerical solutions of path-conservative scheme for Test 6..

The numerical results indicate that the proposed scheme can effectively capture the corresponding shock waves without producing non-physical results, whether using the HLLC solver or LSRS method as the numerical flux. Additionally, the results suggest that there is no apparent difference between these two fluxes, likely because both solvers are constructed based on the constant φ. We also present the energy errors of the numerical solutions obtained with the Lax-Friedrichs scheme, denoted as *Ref* in the figure. For all three methods, the grid size is set to $1/1000$ in the computation of energy errors. The results indicate that, although the energy errors of the path-conservative schemes accumulate over time, they remain within an acceptable range and are consistently equal to or smaller than those of the Lax-Friedrichs scheme.

7.2. One-dimensional moving elastic-plastic interface problem

This subsection includes two examples involving leftward and rightward steady-state elastic-plastic solid interfaces. These examples aim to verify the feasibility of the proposed elastic-plastic transition approach.

Test 3. The initial interface of the steady-state contact discontinuity is located at $x = 2.0$. The wave propagates to the left with a speed of 1. The nondimensional computation ends at time 1. The nondimensional initial conditions are

$$\begin{cases} u_L = -1.0, \quad p_L = 1.0, \quad s_L = -1.0, \quad \rho_L = 2.5 \\ u_R = -1.0, \quad p_R = 1.0, \quad s_R = -2000.0, \quad \rho_R = 2.7 \end{cases}$$

Test 4. The initial interface of the steady-state plastic wave is located at $x = 2.0$. The wave propagates to the right with a speed of 1. The nondimensional computation ends at time 1. The nondimensional initial conditions are

$$\begin{cases} u_L = 1.0, \quad p_L = 1.0, \quad s_L = -2000.0, \quad \rho_L = 2.9 \\ u_R = 1.0, \quad p_R = 1.0, \quad s_R = -1.0, \quad \rho_R = 2.7 \end{cases} \tag{7.1}$$

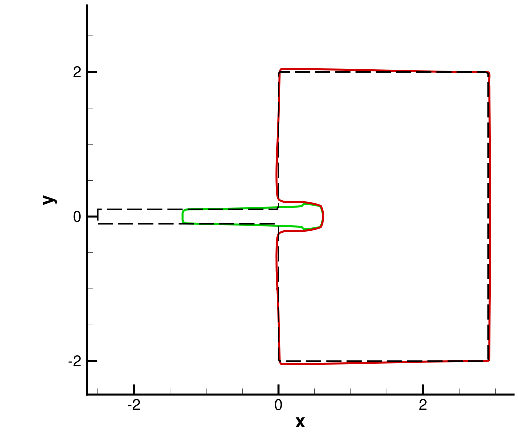

(a) Initial configuration (Black); Post-penetration iron block (Red); Post-penetration iron bar (Green)

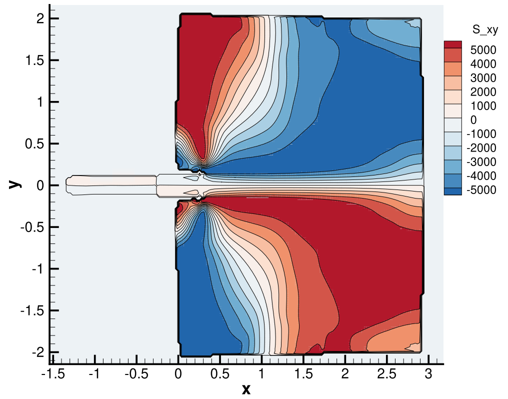

(b) Shear stress

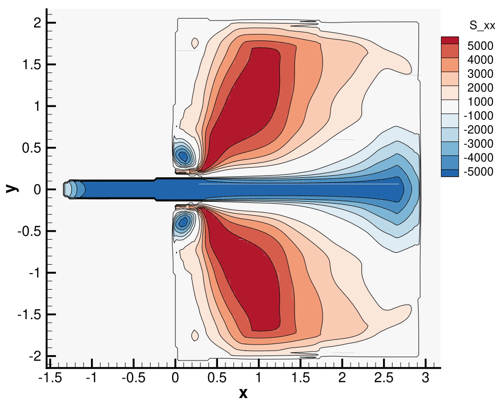

(c) X-direction deviator stress

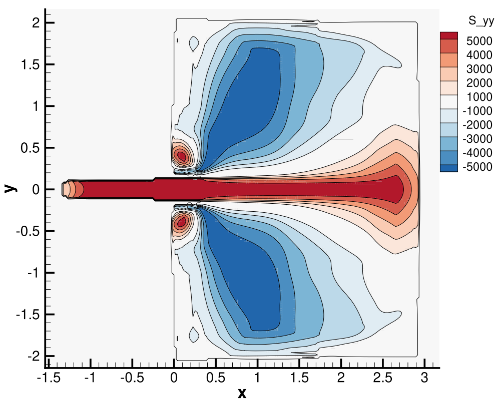

(d) Y-direction deviator stress

Fig. 14. The numerical solutions of path-conservative scheme for Test 7.

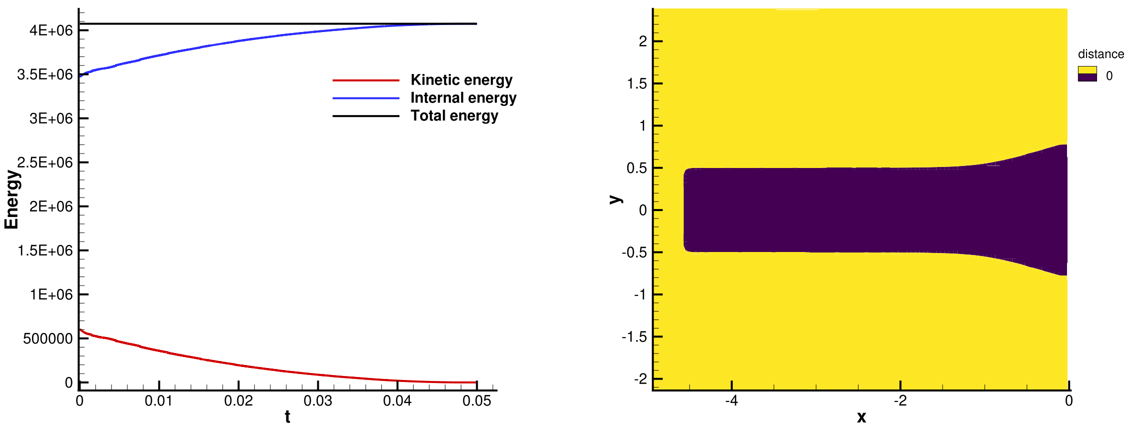

Fig. 15. Two-dimensional Taylor bar impact (test 8).

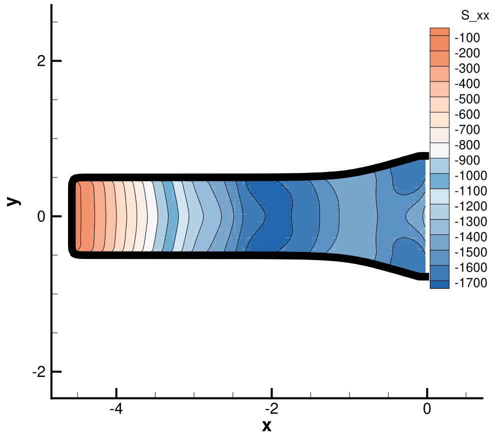

(a) X-direction deviator stress

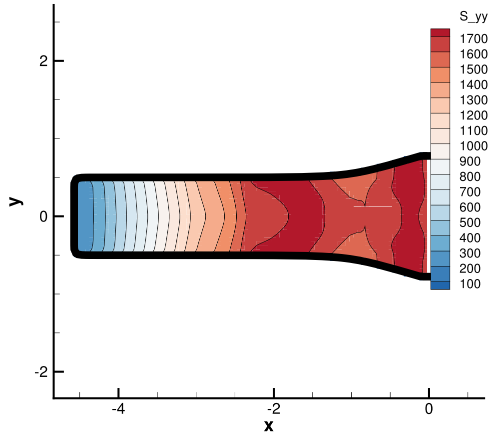

(b) Y-direction deviator stress

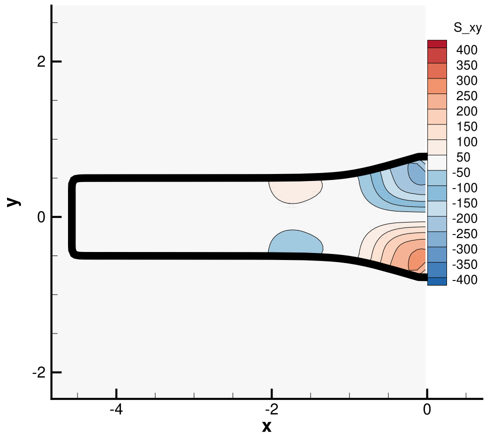

(c) Schematic diagram of shear stress

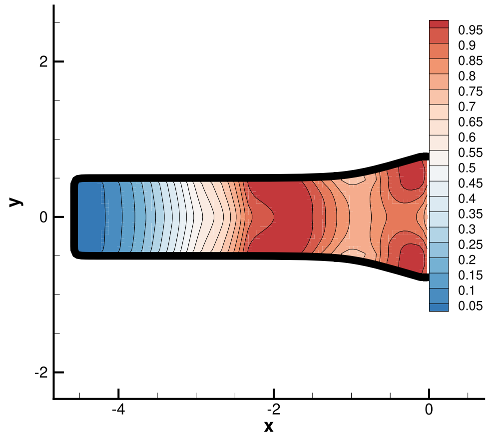

(d) Schematic diagram of elastic-plastic transition

Fig. 16. The numerical solutions of path-conservative scheme for Test 8.

Figs. 8 and 9 present the density, stress, deviatoric stress, and velocity profiles. We can easily derive the exact solutions for these two problems. The numerical results demonstrate that the methods proposed in this paper effectively capture both leftward and rightward propagating elastic-plastic contact discontinuities, highlighting the effectiveness of the proposed methods for the elastic-plastic transitions. Additionally, we computed the L_1-errors for the **PC-HLLC** method and the **PC-LSRS** method, as shown in Table 1. The results indicate that the **PC-LSRS** method exhibits lower errors compared to the **PC-HLLC** method.

7.3. One dimensional elastic-plastic problem

This subsection introduces more intense collisions, causing the solid to undergo elastic-plastic transitions. Through this example, we aim to test whether the numerical methods presented in this paper can accurately capture both elastic and plastic waves.

Test 5. An initial strong collision occurs at the interface $x_0 = 2.0$, causing the elastic and plastic waves to propagate successively to both sides of the interface. The calculation end time is set to 0.002. The nondimensional initial conditions are

$$\begin{cases} u_L = 5.0, \quad \mathrm{p}_L = 1.0, \quad \mathrm{s}_L = 0.0, \quad \rho_L = 2.7 \\ u_R = -5.0, \quad \mathrm{p}_R = 1.0, \quad \mathrm{s}_R = 0.0, \quad \rho_R = 2.7 \end{cases}$$

Figs. 10 and 11 display the density, stress, deviatoric stress, and velocity profiles. In Fig. 10, we use 1000 cells, whereas Fig. 11 utilizes 3000 cells. Fig. 11 demonstrates that, with mesh refinement, our method can more accurately capture elastic and plastic waves. The numerical results illustrate that the proposed scheme effectively captures both elastic and plastic waves.

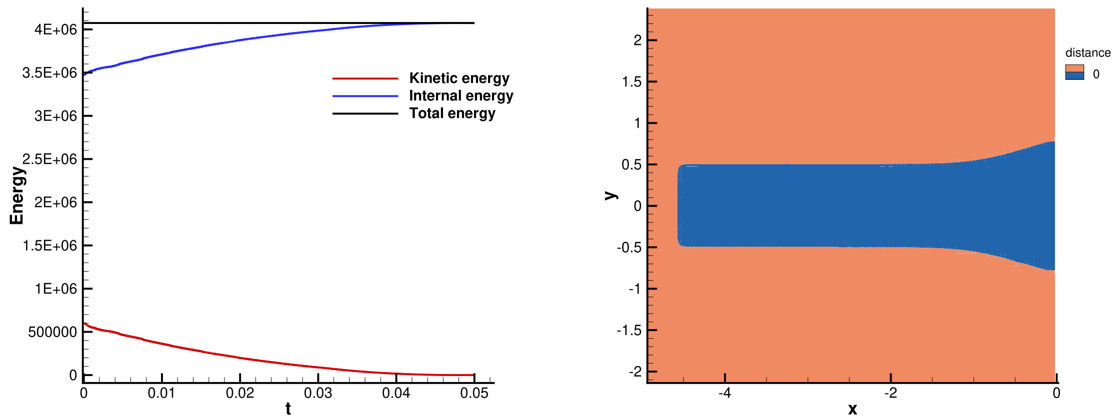

(a) Balance of kinetic, internal and total energy versus time (b) Equipotential surfaces where the distance function equals zero

Fig. 17. Two-dimensional Taylor bar impact with the Jaumann correction (test 9).

Test 6. We further investigate the variation of total energy during elastic-plastic loading and unloading. The initial conditions are

$$\begin{cases} u_L = -1.0, \quad p_L = -100.0, \quad s_L = -2000.0, \quad \rho_L = 2.7, \quad x \in [0.0, 1.6] \\ u_{midleft} = -1.0, \quad p_{midleft} = 1400.0, \quad s_{midleft} = -2000.0, \quad \rho_{midleft} = 2.7, \quad x \in (1.6, 2.0] \\ u_{midright} = 1.0, \quad p_{midright} = 2400.0, \quad s_{midright} = -1800.0, \quad \rho_{midright} = 2.7, \quad x \in (2.0, 2.4] \\ u_R = -1.0, \quad p_R = -100.0, \quad s_R = -1800.0, \quad \rho_R = 2.7, \quad x \in (2.4, 4.0] \end{cases}$$

$$u = 15.0, \mathrm{v} = 0.0, \mathrm{p} = 10^{-11}, \mathrm{s}_{xx} = \mathrm{s}_{yy} = \mathrm{s}_{xyL} = 0.0, \rho = 2.7.$$

Fig. 12 illustrates the elastic and plastic regions at different time instants for Test 6. On the left part of the domain, the solid unloads from a plastic state to an elastic state, while on the right part it loads from an elastic state to a plastic state. It can be observed that both types of transitions–elastic to plastic and plastic to elastic–occur in certain cells. The corresponding numerical solutions are shown in Fig. 13, which demonstrate good agreement with the reference solutions. We focus on the energy errors under multiple elastic-plastic transitions, displayed in Fig. 13(d). The results indicate that the relative energy error remains small, around 1 %.

7.4. Single medium penetration

Test 7. This test involves the penetration of a single medium, where an iron bar impacts an iron block. The nondimensionalization parameters for iron are $\gamma = 2.17$, $c_0 = 4600.0$, $\rho_0 = 7.9$, $\mu = 853000$, $Y_0 = 9790.0$ (the yield strength of the material in simple tension) [34]. The entire non-dimensional computational domain is a square region $x \times y \in [-4.0, 4.0] \times [-4.0, 4.0]$, comprising a rectangular region $x \times y \in [-2.5, 0.0] \times [-0.1, 0.1]$ for the left iron bar and a rectangular region $x \times y \in [0.0, 2.9] \times [-2.0, 2.0]$ for the right iron block at the time $t = 0$. A total of 300×300 uniform grid points are distributed in the whole computational domain. The CFL is set to be 0.1, and the non-dimensional terminal time is 0.01. The boundaries are determined by the three level set functions and the constant-pressure one-sided Riemann problem. The non-dimensional initial conditions for the penetration are

$$\begin{cases} u_L = 125.0, \mathrm{v}_L = 0.0, \mathrm{p}_L = 1.0, \mathrm{s}_{xxL} = \mathrm{s}_{yyL} = \mathrm{s}_{xyL} = 0.0, \rho_L = 7.86 \\ u_R = 0.0, \mathrm{v}_R = 0.0, \mathrm{p}_R = 1.0, \mathrm{s}_{xxR} = \mathrm{s}_{yyR} = \mathrm{s}_{xyR} = 0.0, \rho_R = 7.86 \end{cases} \tag{7.2}$$

Fig. 14(a) displays the zero equipotential surface of the level set function at the end of the computation. It can be observed that the iron bar has clearly penetrated the iron block. In Fig. 14, the distribution of the x-direction deviatoric stress s_{xx}, y-direction deviatoric stress s_{yy}, and shear stress s_{xy} with the calculation termination time of 0.01 is shown. Although this numerical result does not have an exact solution for comparison, by comparing it with the results given in Reference [14], we can find that the present results, by considering the non-conservative nature of the stress equation, will show more symmetrical numerical results with more contour lines, which shows the advantages of the scheme proposed in this paper. Additionally, the numerical results validate the stability and robustness of the proposed method.

7.5. Taylor bar impacting on a wall

Test 8. This test involves a two-dimensional aluminum Taylor bar impacting a rigid wall, with material parameters for the aluminum consistent with those used in the previous example. The entire non-dimensional computational domain is a square region $x \times y \in [-6, 0] \times [-6, 6]$, and a rectangular region $x \times y \in [-5, 0] \times [-0.5, 0.5]$ for the aluminum Taylor bar at the time $t = 0$. A total of

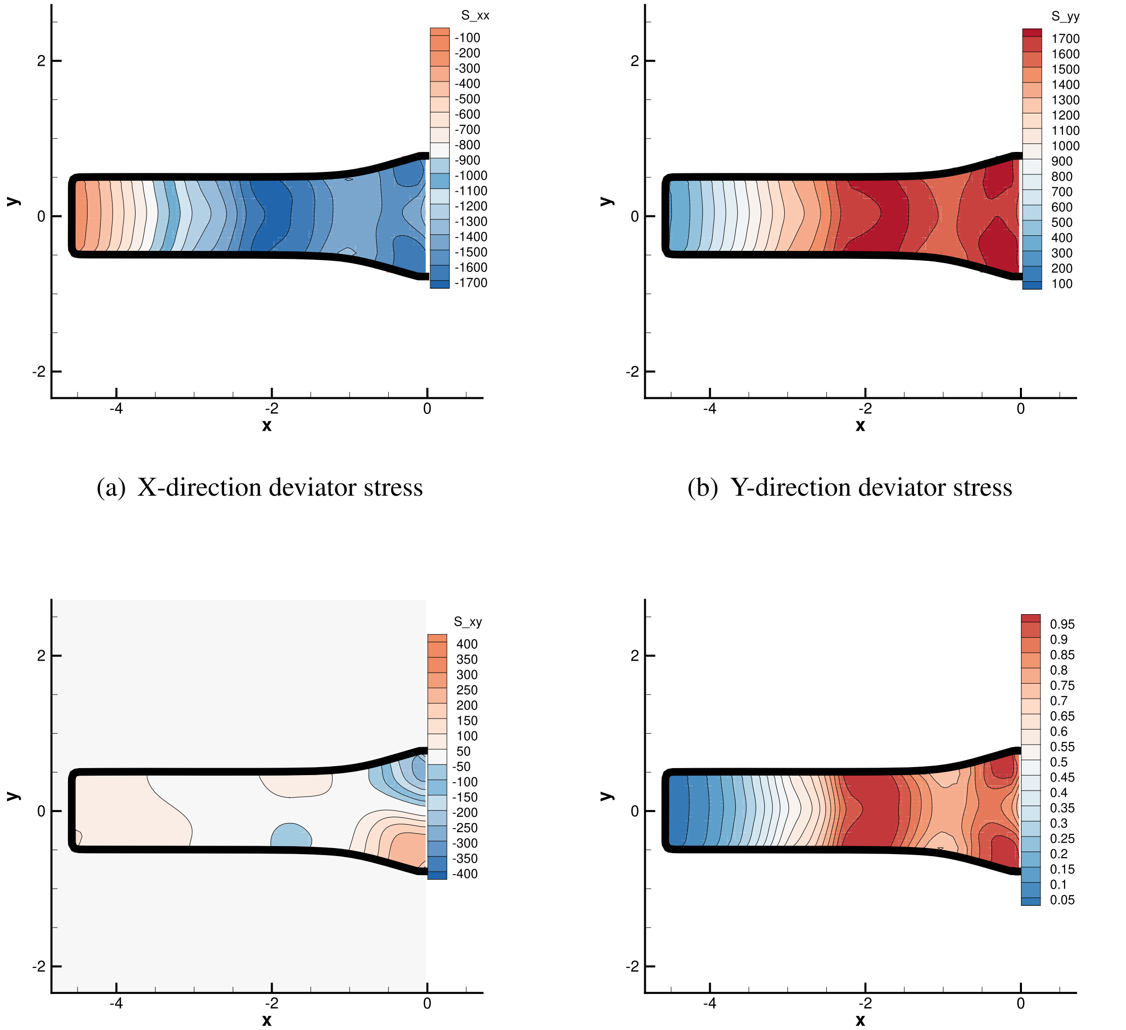

(a) X-direction deviator stress

(b) Y-direction deviator stress

(c) Schematic diagram of shear stress

(d) Schematic diagram of elastic-plastic transition

Fig. 18. The numerical solutions of path-conservative scheme for Test 9.

120×240 uniform grid points are distributed in the whole computational domain. The CFL is set to be 0.1, and the non-dimensional terminal time is 0.05. A wall boundary condition is prescribed for the right boundary while others are determined by the level set function and the constant-pressure one-sided Riemann problem. The non-dimensional initial conditions for the Taylor bar are

Fig. 15(a) illustrates the conversion of the kinetic energy of the Taylor bar into internal energy, thereby maintaining energy conservation and verifying the convergence of the proposed method. Fig. 15(b) displays the zero equipotential surface of the level set function at the end of the calculation, with the final length of the Taylor bar being 4.573 (differs from the value of 4.555 reported in [14]). The results in [39,48–50] indicate that varying constitutive models and computational methods can influence the final length of the Taylor bar. The Stiffened-gas equation of state used in this paper may be "softer" than the Mie-Grüneisen equation of state, resulting in a shorter final length (4.6002 in [50] and 4.605 in [39].). Fig. 16 illustrates the x-direction deviator stress s_{xx}, y-direction deviator stress s_{yy}, shear stress s_{xy} distribution, and the elastic-plastic transition within the Taylor bar, with a value of 1 signifying a plastic state, and a value less than 1 indicating an elastic state. The numerical results in 16 indicate that this paper's method, which accounts for non-conservative properties, provides a more detailed representation of the stress-dependent elastic-plastic transition within the Taylor bar. In addition, numerical results prove that the two-dimensional expansion method is trustworthy.

7.6. Taylor bar impacting on a wall with the Jaumann correction

To evaluate the path-conservative scheme incorporating the Jaumann correction, we recompute the Taylor bar impact on a wall test case, maintaining the same initial conditions as previously set.

The numerical results in Fig. 17(a) show that by the end time, all kinetic energy has been converted into internal energy. Fig. 17(b) illustrates the final shape of the Taylor bar, with a length of 4.574. Fig. 18(a–d) display the corresponding stress components in the x-direction, y-direction, shear stress, and elastic-plastic transition results. We observe that after incorporating the Jaumann correction, the stress contour details indeed change compared to the results in Fig. 16. Additionally, the numerical results indicate that the path-conservative method proposed in this paper can be extended to more complex non-conservative terms.

8. Conclusions

In this work, a path-conservative finite volume scheme for hypo-elastic plastic solids was proposed. This scheme can account for the elastic-plastic transition and effectively couple the non-conservative characteristics of the stress equation by using the path-conservative method. This method constructs a suitable path for the shock wave and demonstrates its compatibility with the physical property of Hooke's law. Moreover, by utilizing the dimension splitting method, we extend the one-dimensional theory to two dimensions, allowing various existing elastic-plastic solid approximate solvers to be logically interpreted within this unified framework. We further extend the two-dimensional work to incorporate the Jaumann correction, demonstrating the robust extensibility of the path-conservative method developed in this paper. Numerical results confirm that the proposed method yields accurate numerical results and provids a more detailed representation of the stress-dependent elastic-plastic transition.

In the future, to enhance the resolution of elastic-plastic transition, the path-conservative discontinuous Galerkin method for one- and high- dimensional elastic-plastic solids will be developed. Furthermore, integrating the non-conservative approach proposed in this paper with a genuinely high-dimensional approximate Riemann solver may better capture the dimensional effects on shear stress. Additionally, we also hope to extend this work to a broader range of elastic-plastic constitutive models, including hyperelastic models, in the future.

Declaration of interests

The authors declare that they have no known competing financial interests or personal relationships that could have appeared to influence the work reported in this paper.

Acknowledgment

This work is supported by the National Natural Science Foundation of China (Grant No.12401697), the Postdoctoral Fellowship Program of the China Postdoctoral Science Foundation under Grant Number GZC20233380, and the Fundamental Research Funds for the Central Universities. We also acknowledge the high-performance computing resources provided by the School of Mathematical Sciences at Beihang University. The work of C.Yu is funded by the Deutsche Forschungsgemeinschaft (DFG, German Research Foundation) - Project number 525853336 – SPP 2410 "Hyperbolic Balance Laws: Complexity, Scales and Randomness."

We would like to express our gratitude to Dr. K. Cao for his valuable discussions related to this article. We also sincerely appreciate the reviewers' comments, which have not only enhanced our understanding of various elastic-plastic models but also provided substantial benefits for improving the paper.

References

[1] X. Garaizar, Solution of a Riemann problem for elasticity, J. Elast. 26 (1) (1991) 43–63.
[2] P. Le Floch, F. Olsson, A second-order Godunov method for the conservation laws of nonlinear elastodynamics, IMPACT Comput. Sci. Eng. 2 (4) (1990) 318–354.
[3] S.L. Gavrilyuk, N. Favrie, R. Saurel, Modelling wave dynamics of compressible elastic materials, J. Comput. Phys. 227 (5) (2008) 2941–2969.
[4] G.H. Miller, P. Colella, A high-order Eulerian Godunov method for elastic-plastic flow in solids, J. Comput. Phys. 167 (1) (2001) 131–176.
[5] P.T. Barton, D. Drikakis, E. Romenski, V.A. Titarev, Exact and approximate solutions of Riemann problems in non-linear elasticity, J. Comput. Phys. 228 (18) (2009) 7046–7068.
[6] J.A. Trangenstein, R.B. Pember, Numerical algorithms for strong discontinuities in elastic-plastic solids, J. Comput. Phys. 103 (1) (1992) 63–89.
[7] W. Boscheri, R. Loubère, P.-H. Maire, A cell-centered Lagrangian ADER-MOOD finite volume scheme on unstructured meshes for a class of hyper-elasticity models, arXiv preprint arXiv:2104.02139 (2021).
[8] M.L. Wilkins, Methods in computational physics, Calcul. Elast.–Plastic Flow (1964) 211–263.
[9] Z. Zeng, W. Yuan, C. Feng, T. Liu, S. Zhang, A genuinely 2D well-balanced method for elastic-plastic flow in cylindrically symmetric coordinates, Adv. Appl. Math. Mech. 17 (2) (2025) 599–632.
[10] F. Zhao, C. Wang, X. Jia, W. Wang, Harten-Lax-van Leer-discontinuities with elastic waves (HLLD-e) approximate Riemann solver for two-dimensional elastic-plastic flows with slip/no-slip interface boundary conditions, Comput. Fluids 265 (2023) 106015.
[11] L. Wang, I.S. Menshov, A.A. Serezhkin, Numerical and analytical investigation of shock wave processes in elastoplastic media, Comput. Math. Math. Phys. 63 (10) (2023) 1860–1873.
[12] I. Peshkov, W. Boscheri, R. Loubere, E. Romenski, M. Dumbser, Theoretical and numerical comparison of hyperelastic and hypoelastic formulations for Eulerian non-linear elastoplasticity, J. Comput. Phys. 387 (2019) 481–521.
[13] I.S. Menshov, A.V. Mischenko, A.A. Serejkin, Numerical modeling of elastoplastic flows by the Godunov method on moving Eulerian grids, Math. Models Comput. Simul. 6 (2) (2014) 127–141.
[14] Z. Zeng, K. Cao, C. Feng, Y. Wang, T. Liu, A genuinely two-dimensional approximate Riemann solver with stress continuity for hypo-elastic solids, Commun. Comput. Phys. 36 (4) (2024) 1113–1155.
[15] R. Abgrall, How to prevent pressure oscillations in multicomponent flow calculations: a quasi conservative approach, J. Comput. Phys. 125 (1) (1996) 150–160.
[16] K.-M. Shyue, An efficient shock-capturing algorithm for compressible multicomponent problems, J. Comput. Phys. 142 (1) (1998) 208–242.
[17] R. Saurel, R. Abgrall, A simple method for compressible multifluid flows, SIAM J. Scient. Comput. 21 (3) (1999) 1115–1145.
[18] J. Cheng, F. Zhang, T. Liu, A quasi-conservative discontinuous Galerkin method for solving five equation model of compressible two-medium flows, J. Sci. Comput. 85 (1) (2020) 12.

[19] C. Parés, Numerical methods for nonconservative hyperbolic systems: a theoretical framework, SIAM J. Numer. Anal. 44 (1) (2006) 300–321.
[20] R. Abgrall, S. Karni, A comment on the computation of non-conservative products, J. Comput. Phys. 229 (8) (2010) 2759–2763.
[21] T.Y. Hou, P.G. LeFloch, Why nonconservative schemes converge to wrong solutions: error analysis, Math. Comput. 62 (206) (1994) 497–530.
[22] K. Xu, Z. Gao, Z. Qian, C. Jiang, C.-H. Lee, Numerical path preserving Godunov schemes for hyperbolic systems, J. Comput. Phys. (2023) 112297.
[23] H. Wang, H. Zhu, Z. Gao, A bound-and positivity-preserving path-conservative discontinuous Galerkin method for compressible two-medium flows, J. Comput. Phys. 529 (2025) 113867.
[24] J. Cheng, F. Zhang, A bound-preserving and positivity-preserving path-conservative discontinuous Galerkin method for solving five-equation model of compressible two-medium flows, SIAM J. Scient. Comput. 44 (4) (2022) B1195–B1220.
[25] G.D. Maso, P.G. Lefloch, F. Murat, Definition and weak stability of nonconservative products, J. Mathématiques Pures et Appliqués 74 (6) (1995).
[26] M.L. Munoz-Ruiz, C. Pares, Godunov method for nonconservative hyperbolic systems, ESAIM-Math. Modell. Numer. Analy.-Model. Mathematique et Analyse Numerique 41 (1) (2007) 169–185. https://doi.org/10.1051/m2an:2007011
[27] L. Wang, I.S. Menshov, A.A. Serezhkin, Numerical and analytical investigation of shock wave processes in elastoplastic media, Comput. Math. Math. Phys. 63 (10) (2023) 1860–1873. https://doi.org/10.1134/S0965542523100135
[28] I. Toumi, A weak formulation of Roe's approximate Riemann solver, J. Comput. Phys. 102 (2) (1992) 360–373.
[29] S. Gao, T. Liu, A solution structure-based adaptive approximate (SSAA) Riemann solver for the elastic-perfectly plastic solid, Commun. Comput. Phys. 25 (3) (2019) 781–811.
[30] B.P. Howell, G.J. Ball, A free-Lagrange augmented Godunov method for the simulation of elastic-plastic solids, J. Comput. Phys. 175 (1) (2002) 128–167.
[31] G. Dal Maso, P.G. Le Floch, F. Murat, Definition and weak stability of nonconservative products J. Math. Pures Appl. 74 (1995) 483–548. .
[32] P.D. Lax, Hyperbolic Systems of Conservation Laws and The Mathematical Theory of Shock Waves, SIAM, 1973.
[33] S. Gao, T. Liu, 1D exact elastic-perfectly plastic solid Riemann solver and its multi-material application, Adv. Appl. Math. Mech. 9 (3) (2017) 621–650.
[34] S. Gao, T. Liu, C. Yao, A complete list of exact solutions for one-dimensional elastic-perfectly plastic solid Riemann problem without vacuum, Commun. Nonlinear Sci. Numer. Simul. 63 (2018) 205–227.
[35] M.J. Castro Díaz, E.D. Fernández-Nieto, T. Morales de Luna, G. Narbona-Reina, C. Parés, A HLLC scheme for nonconservative hyperbolic problems. application to turbidity currents with sediment transport, ESAIM: Math. Modell. Numer. Anal. 47 (1) (2013) 1–32.
[36] Z. Zeng, C. Feng, C. Yu, T. Liu, Linearized double-shock approximate Riemann solver for augmented linear elastic solid, Numer. Math. Theory, Methods Appl. 15 (1) (2022).
[37] R. Li, Y. Wang, C. Yao, A robust Riemann solver for multiple hydro-elastoplastic solid mediums, arXiv preprint arXiv:1902.05145 (2019).
[38] J.-B. Cheng, L. Liu, S. Jiang, M. Yu, Z. Liu, A second-order cell-centered Lagrangian scheme with a HLLC Riemann solver of elastic and plastic waves for two-dimensional elastic-plastic flows, J. Comput. Phys. 413 (2020) 109452.
[39] X. Li, J. Zhai, Z. Shen, An HLLC-type approximate Riemann solver for two-dimensional elastic-perfectly plastic model, J. Comput. Phys. 448 (2022) 110675.
[40] D. Fridrich, R. Liska, B. Wendroff, Cell-centered Lagrangian Lax–Wendroff HLL hybrid method for elasto-plastic flows, Computers & Fluids 157 (2017) 164–174.
[41] T. Heuzé, Lax-Wendroff schemes for elastic-plastic solids, J. Comput. Phys. 396 (2019) 89–105.
[42] Q. Chen, L. Li, J. Qi, Z. Zeng, B. Tian, T. Liu, A cell-centered Lagrangian scheme with an elastic-perfectly plastic solid Riemann solver for wave propagations in solids, Adv. Appl. Math. Mech. 14 (2022) 703–724.
[43] L. Wang, I.S. Menshov, A.A. Serezhkin, Numerical modelling of large elasto-plastic multi-material deformations on Eulerian grids, Russian J. Numer. Anal. Math. Modell. 39 (3) (2024) 165–174.
[44] J.R. West, M.C. Adler, S.K. Lele, A high-order, localized-artificial-diffusivity method for Eulerian simulation of multi-material elastic-plastic deformation with strain hardening, J. Comput. Phys. 514 (2024) 113205.
[45] Z. Zeng, C. Feng, X. Zhang, S. Zhang, T. Liu, A genuinely two-dimensional HLL-Type approximate Riemann solver for hypo-elastic plastic flow, Commun. Comput. Phys. 34 (2) (2023) 318–356.
[46] A. Serezhkin, HLLEPJ and HLLCEPJ Riemann solvers for the Wilkins model of elastoplasticity, J. Comput. Phys. 492 (2023) 112419.
[47] J.-B. Cheng, Y. Jia, S. Jiang, E.F. Toro, M. Yu, A second-order cell-centered Lagrangian method for two-dimensional elastic-plastic flows, Commun. Comput. Phys. 22 (5) (2017) 1224–1257.
[48] P.-H. Maire, R. Abgrall, J. Breil, R. Loubère, B. Rebourcet, A nominally second-order cell-centered Lagrangian scheme for simulating elastic-plastic flows on two-dimensional unstructured grids, J. Comput. Phys. 235 (2013) 626–665.
[49] E.J. Lieberman, X. Liu, N.R. Morgan, D.J. Luscher, D.E. Burton, A higher-order Lagrangian discontinuous Galerkin hydrodynamic method for solid dynamics, Comput. Methods Appl. Mech. Eng. 353 (2019) 467–490.
[50] P. Niu, F. Qing, C. Wang, Z. Jia, W. Wang, An efficient second-order cell-centered Lagrangian discontinuous Galerkin method for two-dimensional elastic-plastic flows, Phys. Fluids 36 (3) (2024).